Experimental Gerontology 130 (2020) 110784

Contents lists available at ScienceDirect

Experimental Gerontology

journal homepage: www.elsevier.com/locate/expgero

Long term breeding of the *Lmna G609G* progeric mouse: Characterization of homozygous and heterozygous models

Anna Zaghini[a], Giuseppe Sarli[a], Catia Barboni[a], Mara Sanapo[a], Valeria Pellegrino[a], Alessia Diana[a], Nikolina Linta[a], Julie Rambaldi[a], Maria Rosaria D'Apice[b], Michela Murdocca[c], Massimiliano Baleani[d], Fabio Baruffaldi[d], Roberta Fognani[d], Rosaria Mecca[d], Anna Festa[d], Serenella Papparella[e], Orlando Paciello[e], Francesco Prisco[e], Cristina Capanni[f,g], Manuela Loi[f,g], Elisa Schena[f,g], Giovanna Lattanzi[f,g], Stefano Squarzoni[f,g,*]

[a] Department of Veterinary Medical Sciences, University of Bologna, Ozzano Emilia, Bologna, Italy
[b] Medical Genetics Laboratory, Tor Vergata Hospital, Rome, Italy
[c] Department of Biomedicine and Prevention, University of Rome "Tor Vergata", Rome, Italy
[d] IRCCS Istituto Ortopedico Rizzoli, Medical Technology Laboratory, Bologna, Italy
[e] Department of Veterinary Medicine and Animal Production, University of Naples Federico II, Naples, Italy
[f] CNR - Institute of Molecular Genetics "Luigi Luca Cavalli-Sforza"- Unit of Bologna, Bologna, Italy
[g] IRCCS Istituto Ortopedico Rizzoli, Bologna, Italy

ARTICLE INFO

Section Editor: Werner Zwerschke

Keywords:
Aging
Hutchinson-Gilford Progeria Syndrome (HGPS)
Animal model breeding
Bone strength
Kyphosis
Quality of life

ABSTRACT

The transgenic *Lmna*^{G609G} progeric mouse represents an outstanding animal model for studying the human Hutchinson-Gilford Progeria Syndrome (HGPS) caused by a mutation in the *LMNA* gene, coding for the nuclear envelope protein Lamin A/C, and, as an important, more general scope, for studying the complex process governing physiological aging in humans. Here we give a comprehensive description of the peculiarities related to the breeding of *Lmna*^{G609G} mice over a prolonged period of time, and of many features observed in a large colony for a 2-years period. We describe the breeding and housing conditions underlining the possible interference of the genetic background on the phenotype expression. This information represents a useful tool when planning and interpreting studies on the *Lmna*^{G609G} mouse model, complementing any specific data already reported in the literature about this model since its production. It is also particularly relevant for the heterozygous mouse, which mirrors the genotype of the human pathology however requires an extended time to manifest symptoms and to be carefully studied.

Abbreviations

HGPS Hutchinson-Gilford Progeria Syndrome
LamA/C lamin A/C

1. Introduction

1.1. The mutated protein

Lamin A/C (LamA/C) is a major component of the nuclear lamina, a three-dimensional matrix lining the internal surface of the inner nuclear membrane. LamA/C is important for maintaining the nuclear structure (Moir and Spann, 2001) and it governs many key nuclear functions such as chromatin organization, DNA replication, transcription, DNA repair and cell-cycle progression (Lopez-Soler et al., 2001; Prokocimer et al., 2013). Mutations in the LamA/C gene (*LMNA*) give rise to a group of rare diseases collectively called laminopathies and distinguished in "tissue-specific" or "systemic" forms. Tissue-specific laminopathies affect predominantly one tissue type (skeletal or cardiac muscle, adipose tissue etc.), systemic laminopathies affect globally the organism, which always shows more or less marked premature aging traits (Camozzi et al., 2014). The most representative disease among systemic laminopathies is the Hutchinson-Gilford Progeria Syndrome (HGPS, OMIM 176670).

1.2. The Hutchinson-Gilford Progeria Syndrome

HGPS is a rare, dominant genetic disorder characterized by

* Corresponding author at: CNR - Institute of Molecular Genetics "Luigi Luca Cavalli-Sforza" - Unit of Bologna, Bologna, Italy.
E-mail address: stefano.squarzoni@cnr.it (S. Squarzoni).

https://doi.org/10.1016/j.exger.2019.110784
Received 12 June 2019; Received in revised form 26 October 2019; Accepted 15 November 2019
Available online 30 November 2019
0531-5565/ © 2019 The Authors. Published by Elsevier Inc. This is an open access article under the CC BY-NC-ND license (http://creativecommons.org/licenses/BY-NC-ND/4.0/).

accelerated aging, bone resorption (particularly at phalanges, clavicles and mandible), skin and adipose tissue atrophy and atherosclerosis (Mounkes and Stewart, 2004). The onset is in the first year of life and patients die at an average age of 14.5 years, predominantly from atherosclerosis and myocardial infarction or stroke (Merideth et al., 2008; González and Andrés, 2011). The majority of HGPS patients carry in heterozygosis a de novo point mutation (c.1824C > T; p.G608G) which creates a cryptic splice site in exon 11, resulting in a mutant form of prelamin A, the LamA/C precursor protein. The aberrant protein, named progerin, is permanently farnesylated and carboxymethylated at its C-terminal domain, displays altered structure and biochemical properties with respect to prelamin A (De Sandre-Giovannoli et al., 2003; Eriksson et al., 2003; Meta et al., 2006) and cannot undergo any further processing towards mature LamA/C.

1.3. The murine model

The transgenic *Lmna*^{G609G} knock-in mouse model for the human HGPS was generated in 2011 by C. López-Otín (Osorio et al., 2011). Mice carrying this mutation express lamin A, lamin C, and progerin, reproducing the protein expression pattern of HGPS patients. This transgenic mouse has the characteristic signs of progeroid models and phenocopies the main clinical manifestations of human HGPS, including impaired somatic growth, skeletal anomalies such as kyphosis, mandible hypoplasia, malocclusion, skin and adipose tissue atrophy, cardiovascular alterations and shortened life span. A depletion of vascular smooth muscle cells (VSMCs) in the aortic arch but not in the thoracic aorta was demonstrated in the homozygous animal (Osorio et al., 2011). Cardiovascular alterations affecting heterozygous *Lmna*$^{G609G/+}$ mice have been further described in detail, including vessel stiffening (Del Campo et al., 2019) (Kim et al., 2018) and atherosclerosis when mice are crossed with Apoe-null mice (Hamczyk et al., 2018), excessive aortic calcification and in an impaired ability of primary aortic vascular smooth muscle cells to inhibit vascular calcification (Villa-Bellosta et al., 2013). Findings from previous studies indicate that mice and humans may show different sensitivity to progeria-causing alterations, and these differences should be carefully taken into consideration to interpret results obtained in murine models (Osorio et al., 2009).

2. Results and discussion

2.1. Housing and breeding

The maintenance of the colony was guaranteed by 37 dams (7 *Lmna*$^{+/+}$ and 30 *Lmna*$^{G609G/+}$) and 25 males *Lmna*$^{G609G/+}$ over a 2-year period of study. The colony was maintained inbred and reached 8 generations producing a total of 282 pups. At weaning, genomic analysis of *Lmna* exon 11 and LamA/C and progerin expression assessment (Fig. 1) as well as headset marking were performed.

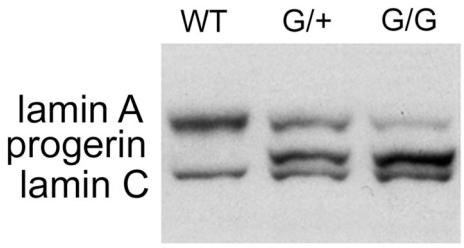

Fig. 1. LamA/C and Progerin expression (Western blot analysis). WT: wild type; G/+: heterozygous; G/G: homozygous.

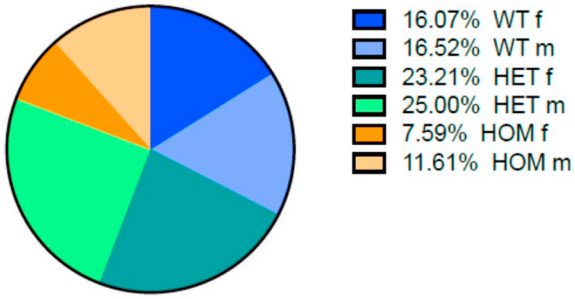

Fig. 2. Pie chart. Genotype and sex of pup born from heterozygous mating. Wt = Lmna$^{+/+}$ n° 92/282; Hom = Lmna$^{G609G/G609G}$ n° 54/282; Het = Lmna$^{G609G/+}$ n° 136/282; f = females; m = males.

2.2. Nest and breeding characterization

Genotype and sex of pups born from mating heterozygous-x-heterozygous and Wt-x-heterozygous are shown in Fig. 2, respectively: 32.59% of the weaned pups were WT, 48.21% heterozygous and 19.2% homozygous. When heterozygous were mated with WT mice, pups were 36.21% WT and 63.80% heterozygous. In the second type of mating, heterozygous mice were more than expected from Mendelian's proportions, while in the first type of mating homozygous mice were less and WT were more compared to expectations. For both genotypes, mice carrying the mutation were mostly male. Therefore, it is probable that in some cases females carrying the mutation might have died in utero. The female:male ratio was 1:1.13 for homozygous and 1:1.53 for heterozygous.

2.3. Fertility

Dams delivered the first successful litter starting from 57 days. Between births, a mean of 36 days and 39 days was registered for LmnaG609G/+ and Lmna+/+ females, respectively, which is longer than the 19 days, usual for C75BL/6. No successive litters were observed during the prolonged lactation: we hypothesize that litters born in this period went lost, probably due to the fact that the dams did not have enough milk to feed all pups. Weaning of pups was extended from the classic 21 to 30 days, because a slow growth was observed. Our hypothesis that *Lmna*$^{+/+}$ would be better dams compared to *Lmna*$^{G609G/+}$ was not confirmed. In fact, both genotypes had an average of 2 litters during their reproductive life (range 1–4). Litter size were highly variable, ranging from 1 to 11 pups, however, for both genotypes, the average was 6 pups for each litter, which is more than reported for C57BL/6. Therefore, heterozygous males and females revealed to be reliable breeders. On the other hand, one of the two homozygous females in reproduction was never pregnant, while the second one got pregnant but died during premature delivery, together with fetuses. The homozygous male in reproduction did not succeed in impregnating two fertile heterozygous females. In light of this result and since generally mice reach sexual maturity at about 60 days of age, which is an already senescent age for homozygous, *Lmna*$^{G609G/G609G}$ transgenic mice cannot be considered as breeders. This result agrees with recent data reporting a condition of subfertility for G609G mice related to their general health state more than to defective fertilization (Balmus et al., 2018). In this sense they are not always infertile as reported previously (Osorio et al., 2011). The total pre-weaning pup mortality was around 31%. This rate is in accordance with previous studies conducted on C57BL/6 mice (Weber et al., 2013), even though mortality varies greatly among different studies (Weber et al., 2016). Mouse pups are very sensitive to hypothermia (Weber et al., 2016), moreover, animal models of laminopathies have been proven to benefit from higher temperatures (Liao et al., 2016). So, providing dams with appropriate nesting material is very important to reduce pup mortality

since maternal behavior, including nest building attitude, was not impaired. However, some pup deaths in the first few days after birth likely went unnoticed, since dams often scavenge dead pups. Furthermore, we left periparturient females undisturbed, which may have prevented the discovery of pup loss. In some case rejection or cannibalism of the litter were observed, probably due to the lack of breast milk evidenced by the absence of "milk spot" in some of the dead pups. Such deaths commonly occurred by 1 or 2 days of age. Since birth, transgenic pups had a slower growth in comparison to $Lmna^{+/+}$, suggesting lengthening the weaning period to 30 days. This strategy resulted successful, and no post-weaning mortality was registered. No complication was registered as a consequence of headset marking.

2.4. Behavior - colony health surveillance and animal monitoring

C57BL/6 mice are reported as "touchy" (Baumans, 2005), however no aggressive behavior was ever seen towards the operators and mice were tame when manipulated. Few aggressive behaviors were observed between cage mates, seen only between males fighting to form a hierarchy, especially after cage change. This behavior could be limited by adding some old litter or paper tissue from the old cage into the new one. The weak territorial behavior made it possible to cage males in groups up to 4 animals. Fight wounds were rarely observed, and healed quickly without complications after proper disinfection with iodinate solution. Behavior-associated hair loss, known as barbering (Fig. 3), includes plucking off hairs or whiskers from cage mates (hetero-barbering) or on self (self-barbering), and is common in mice (Kalueff et al., 2006). It occurs often in C57BL/6 appearing to be linked to a form of dominance in which animals co-operate (van den Broek et al., 1993). In cages overpopulated with pups from different litters, barbering of suckling pups by their parents was common (Fig. 3) and, after weaning, the fur in areas with barbering grew normally. No barbering was observed among breeding pairs, neither in lactating mice performed by suckling pups. Barbering has also been negatively correlated with aggressiveness or interpreted as an obsessive-compulsive grooming disorder, representing a stress-evoked response that can be limited with environmental enrichment. In our colony, adult mice displayed barbering in 12% of the cases, less than reported for C57BL/6 in other studies (Long, 1972). Barbering behavior was not related to the genotype and all animals with barbering had healthy skin. Most frequent areas of hair loss were neck, dorsum, snout and head (the last two incompatible with self-barbering).

Fig. 3. Barbering of suckling pups by their parents. Note the broad skin area exposed. No skin lesions are present.

2.5. Onset of symptoms

No differences in the symptoms related to premature aging, apart from bodyweight and lifespan, were observed between males and females. Following weaning and for the first 5–6 weeks of age, all mice were lively, active, explorative and expressed the typical behavior of the species. When observed in their home cage mice were seen moving around the cage, grooming, eating, drinking and interacting with cage mates. All mice built nests using the suitable material provided (pieces of cloth, egg packaging). Apart from lower weight gain rate (see below), the first clinical signs associated with the progeric syndrome arose at 5–6 weeks of age for $Lmna^{G609G/G609G}$ and at 20–32 weeks of age for $Lmna^{G609G/+}$ and were observed during daily inspection of the animals in their cage. The signs were more evident and severe in homozygous than in heterozygous mice and regarded especially fur and skin, eyes and skeletal apparatus. For both genotypes, periocular alopecia was the first characteristic sign registered, followed by thinning and loss of hairs from the limbs, nose and back. Fragility and loss of hairs were evidenced by their presence on the gloves when animals were handled. Fur was evidently opaque and rough compared to $Lmna^{+/+}$ and showed grey/white stripes (Fig. 4).

The skin appeared thin, dry and sclerotic, and an erythema-like redness was clearly visible, particularly in the ventral area probably due to direct exposure to the litter. Interestingly, ocular signs were very common and included microphthalmia, anophthalmia, opacity of the cornea, being different from those described in human patients who are reported to suffer mainly from refractive errors such as hyperopia or keratopathies caused by dryness of the cornea (Merideth et al., 2008) (Mantagos et al., 2017). They occurred in 50% of homozygous mice (Fig. 5), in 17% of heterozygous and in 3% of WT mice. However C57BL/6 mice have high incidence of microphthalmia and other eye defects, suggesting an influence by the genetic background (Smith et al., 1994) (Fuerst et al., 2007).

Transgenic mice also showed dental anomalies, confirmed by radiological and microCT analysis. Mouse incisors grow throughout life and should get in reciprocal contact in such a way that they grind on each other and on the food, thus maintaining a normal length. If upper and lower incisors are not normally aligned, malocclusion occurs meaning that teeth may grow towards the palate or out of the mouth. Malocclusion has been linked to traumas to the growing teeth (impact on cage metal parts, improper handling, fighting, hard food etc.), also an increased incidence in strains such as C57BL/6 is reported (Burkholder et al., 2012). In our study, we never found malocclusion nor other dental alterations in $Lmna^{+/+}$ mice, while in 13% of homozygous and 8% of heterozygous (Fig. 6) the incisors were splayed apart, thin, long or fractured. This condition was early diagnosed during the twice weekly clinical observation and malnourishment was the first consequence. Hydrocephalus was observed in 2 heterozygous mice. Cleft palate was not observed. Reduced mobility and a "shuffling gait" of the hind limbs were common at increasing age. Dental anomalies, together with the impaired motility, reduced agility in climbing and/or standing to reach food, resulted in feeding difficulty for the affected animals. Consequent weakness and definitive weight loss lead to a severe state of apathy and cachexia, rapidly reaching the Humane Endpoints (HE).

Kyphosis was constantly observed (Fig. 7) and aggravated with age (see below).

Tremors (involuntary rhythmic oscillation of body parts) were observed in 2/40 homozygous mice and 2/157 heterozygous mice but never observed in WT mice. Tremors may be related to a possible hypoglycemic state or derive from a neurological disorder (Louis, 2008). Moderate to severe hypoglycemia, not investigated in this study, was described for homozygotes and heterozygotes at 3 and 8 months of age, respectively (Osorio et al., 2011). However, it is possible that shivering may have been confused with tremors. Since homozygotes and heterozygotes have thin fur and no subcutaneous fat, the shivering could

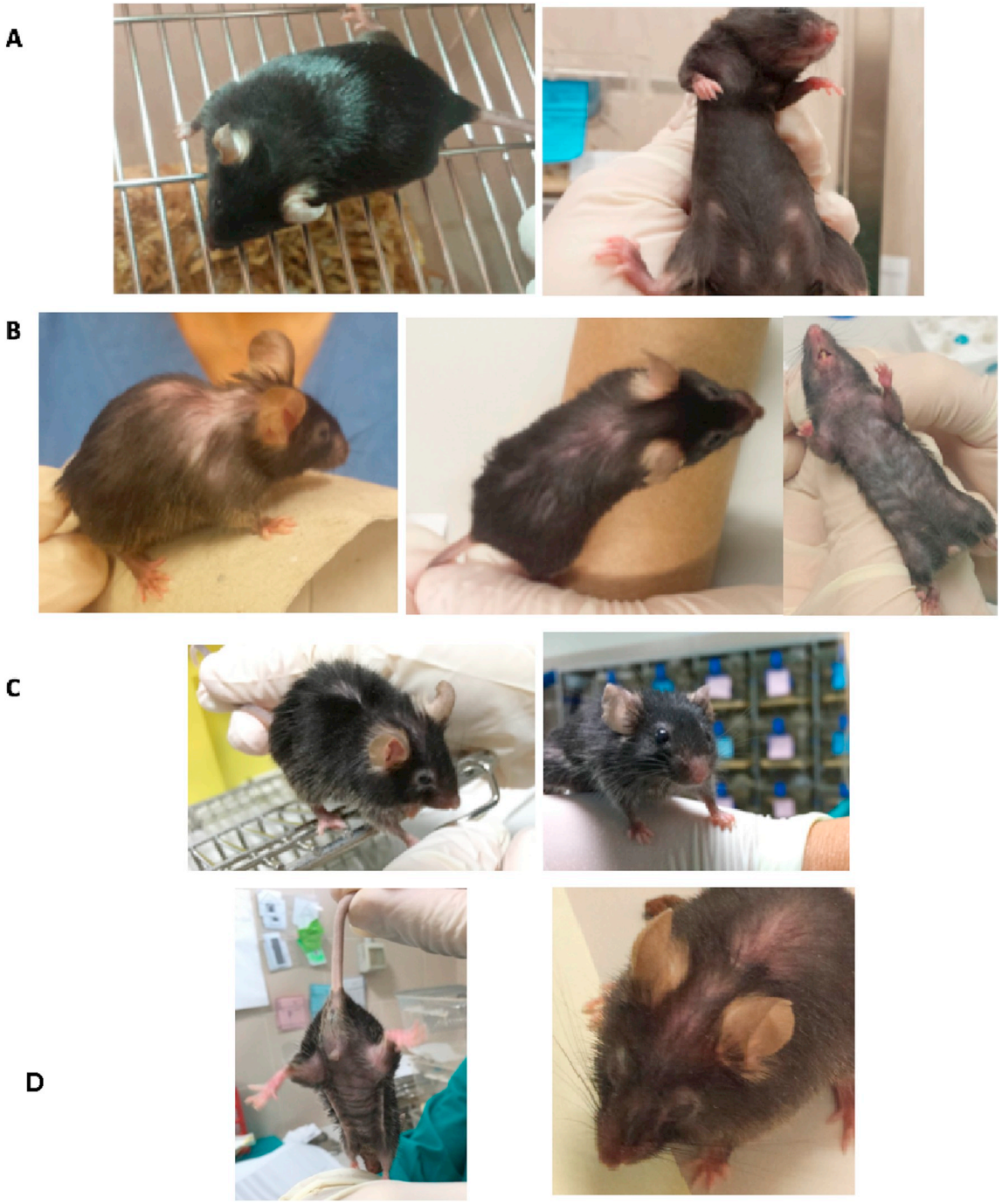

Fig. 4. Fur comparison between *Lmna*$^{+/+}$ mice (A) and *Lmna*^{G609G} transgenic mice (B, C). Note the thick, shiny and glossy fur of the *Lmna*$^{+/+}$ mouse (age 250 days) both in the dorsal and ventral area (A). In contrast, G609G transgenic mice (at ages near to reaching the HE) have sparse and scruffy coat. Trunk hair turned prematurely grey (B). Note the characteristic periocular alopecia (C). These signs were observed in both sexes, in 54/54 homozygous,136/136 heterozygous and in 0/92 WT mice. (D) Thin fur and erythema-like redness.

be a physiological response to hypothermia. Thermoneutrality (30 °C) is reported to improve lifespan of a mouse model of laminopathy, reinforcing the idea that these mice could be more severely influenced by the temperatures commonly used in laboratory animal facilities (Liao et al., 2016).

2.6. Body weight and growth

WT mice grew rapidly reaching a relative plateau weight of 35 g for males and 25 g for females at about 25 weeks. They did not show any weight loss during the study period and were able to reach up to 50 g.

As reported (Osorio et al., 2011), G609G transgenic mice attained lower weights than WT littermates throughout the post-weaning period. The first sign associated with HGPS disease, in fact, includes reduced growth rates. The weight differences were hardly detected at weaning, then between 45 and 48 days of age, mean values of each group began to indicate lower weights for both females and males *Lmna*$^{G609G/+}$ and *Lmna*$^{G609G/G609G}$ (more evident) compared to WT of the same sex (Fig. 8).

In accordance with the first description of these animals, no weight plateau was reached by *Lmna*$^{G609G/G609G}$ animals. Males hardly reached a maximum of 20 g at about 9 weeks of age which was followed by a

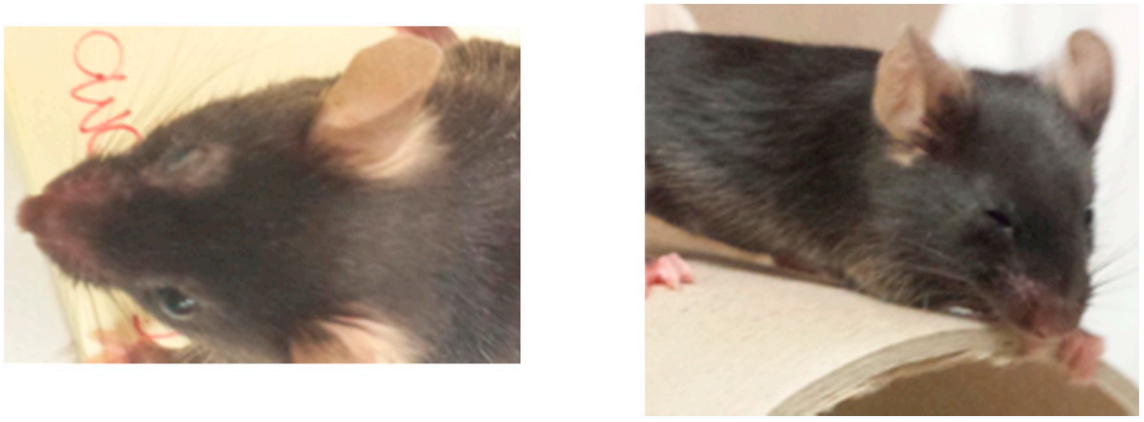

Fig. 5. Ocular signs in *Lmna*^{G609G} transgenic mice. Opacity of the cornea, microphthalmia were observed since weaning in 27/54 homozygote, 23/136 heterozygote and 3/92 WT mice.

rapid weight loss. Heterozygous mice reached a plateau (males *Lmna*$^{G609G/+}$ 28 g; females *Lmna*$^{G609G/+}$ 23 g) at about 20 weeks and maintained this weight until 30 weeks of age, when they progressively started to lose weight.

2.7. Lifespan

The lifespan of *Lmna*^{G609G} transgenic mice is very short compared to a *Lmna*$^{+/+}$. C57BL/6 mice usually survive 18–22 months, females living longer than males. However, longevity is strain specific, depends on several factors and can vary among reports. The oldest *Lmna*$^{+/+}$ mice in our study was a female and lived up to 23 months.

Homozygous mice (n = 15) died prematurely, reaching the humane endpoint at 108 days (Fig. 9). This result is consistent with those reported by previous studies, in which mean lifespan ranges from 103 days to 107 days (Osorio et al., 2011) (Villa-Bellosta et al., 2013). If considered separately, females (n = 8) had a lifespan of 101 days; while males (n = 7) had a lifespan of 115 days. This difference between the two sexes of the same genotype resulted significant (p = 0.01). Heterozygous mice (n = 73), which develop the disease in a less severe way, reached the humane endpoint at 287 days. Osorio (Osorio et al., 2011) and Villa-Bellosta (Villa-Bellosta et al., 2013) reported a mean lifespan of 242 and 238 days, respectively.

Once again females reached the humane endpoint earlier compared to males. In fact, females (n = 40) reached the HE at 266 days, while males (n = 33) at 311 days (p = 8.84e−06). Considering singularly heterozygous dams and virgins we noted that while virgins (n = 30) lived 272 days, dams (n = 10) lived 250 days. Also, means of male lifespan were not affected at all by reproduction and, for both sexes, breeding did not affect lifespan in a significant way. In general, in our

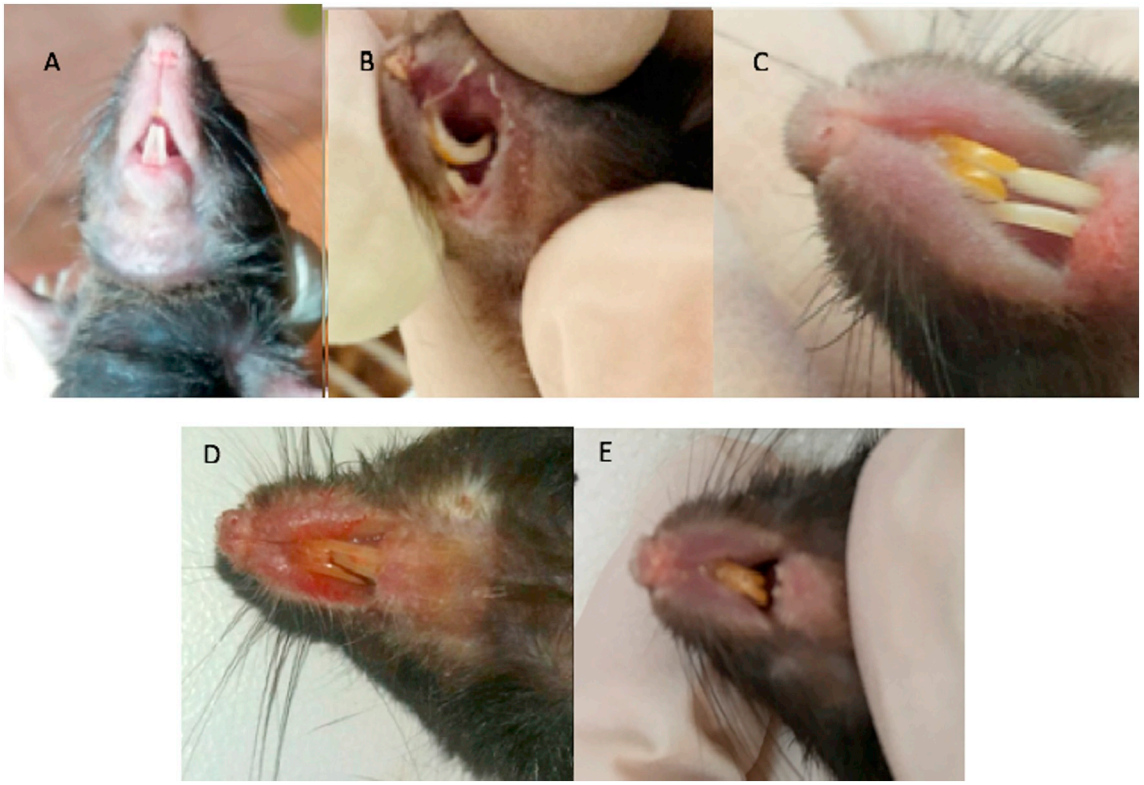

Fig. 6. Dental anomalies. A) Normal teeth, B) Malocclusion, upper incisors extremely curved inwards; C) Long incisors splayed apart; D) Thin, long and fractured incisors; E) Fractured lower incisors and long upper incisors. These defects were observed 7/54 homozygote, 11/136 heterozygote and 0/92 WT mice.

Fig. 7. Kyphosis. Typical *Lmna*^{G609G} transgenic mice kyphosis.

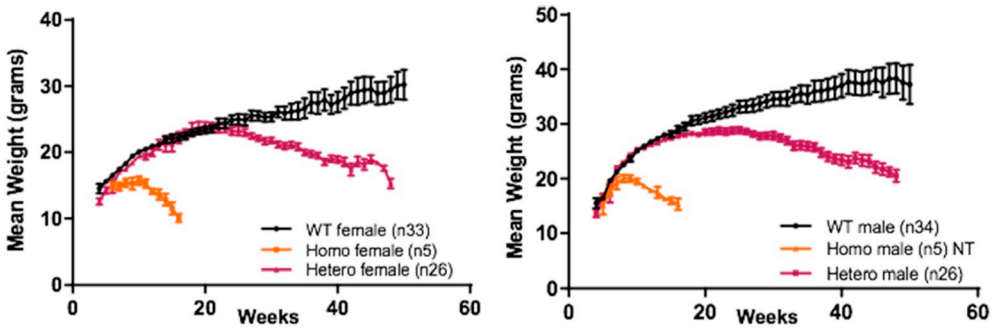

Fig. 8. Body weight plot. Cumulative plot of body weight versus age in females (left) and males (right).

study the mean lifespan of *Lmna*$^{G609G/+}$ was longer than reported in previous studies in which no animal groups larger than 8 individuals were considered (Osorio et al., 2011) (Villa-Bellosta et al., 2013). For this reason, we think that the real mean lifespan of *Lmna*$^{G609G/+}$ we measured could be more reliable. Differences in mean lifespan of mice from the same inbred strains in different environments, demonstrate that life expectancy is influenced not only by genetic factors, but also by the environment. These factors, among others, include diet, temperature and humidity conditions, and husbandry procedures. Obviously, it is likely that genotypes surviving longer are more influenced by environmental factors compared to animals with shorter life. From these results, it appears clear that homozygous are more severely affected by the disease compared to heterozygous mice, and that when using *Lmna*^{G609G} transgenic mice as an animal model to study the effect of drugs on lifespan it would be optimal to consider sex groups separately. Finally, reproduction does not affect lifespan in significant way.

2.8. Feeding boosting

For a subset of mice moistened chow was left on the cage floor, a more accessible position, in order to avoid feeding difficulties. The strategy of adding palatable food on the cage floor is used by many research groups and is part of the *Refinement* principle (Burkholder et al., 2012). In our study, this choice allowed the less motile animals to continue feeding and brought to good results with a general improvement in body weight and life conditions of the affected animals. However, adding moistened chow could be done only for about two weeks after the initial weight loss because longer periods favored abnormal incisors growth that eventually compromised the animal nutrition. Moistened food did not have an impact on lifespan but temporarily improved life quality of mice, thus being considered a valuable refinement strategy that can be used in the case of particular experimental requirements.

2.9. Quality-of-life evaluation

2.9.1. Open Field Test

The Open Field Test (OFT) is not simply a measure of motor activity, but involves other factors such as exploratory drive (curiosity), and fear (anxiety). Mice placed in the center of the arena typically ran to the walled edge then explored their way around the whole arena remaining close to the walls. All mice spent most of the time close to the arena

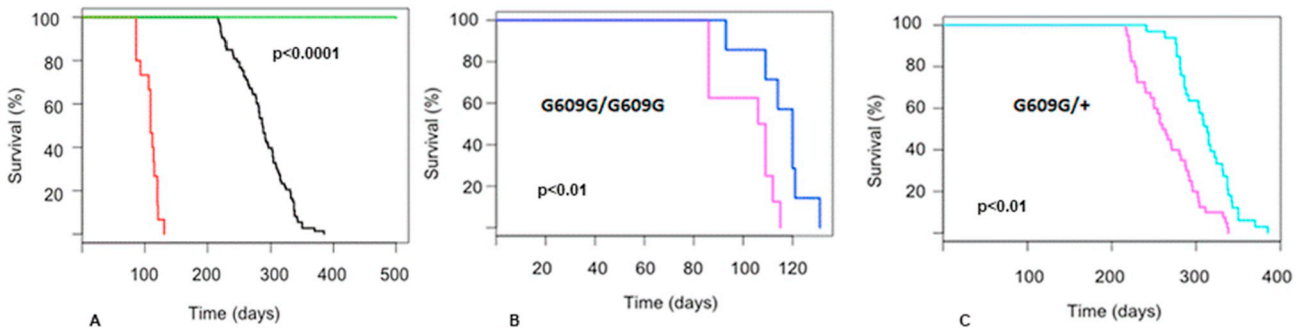

Fig. 9. Life expectancy. A) Kaplan-Meier survival plots for wild type mice (green, $n = 15$), heterozygous mice (black, $n = 73$), and homozygous mice (red, $n = 15$). B) homozygous and C) heterozygous mice: females (pink), and males (blue). (For interpretation of the references to color in this figure legend, the reader is referred to the web version of this article.)

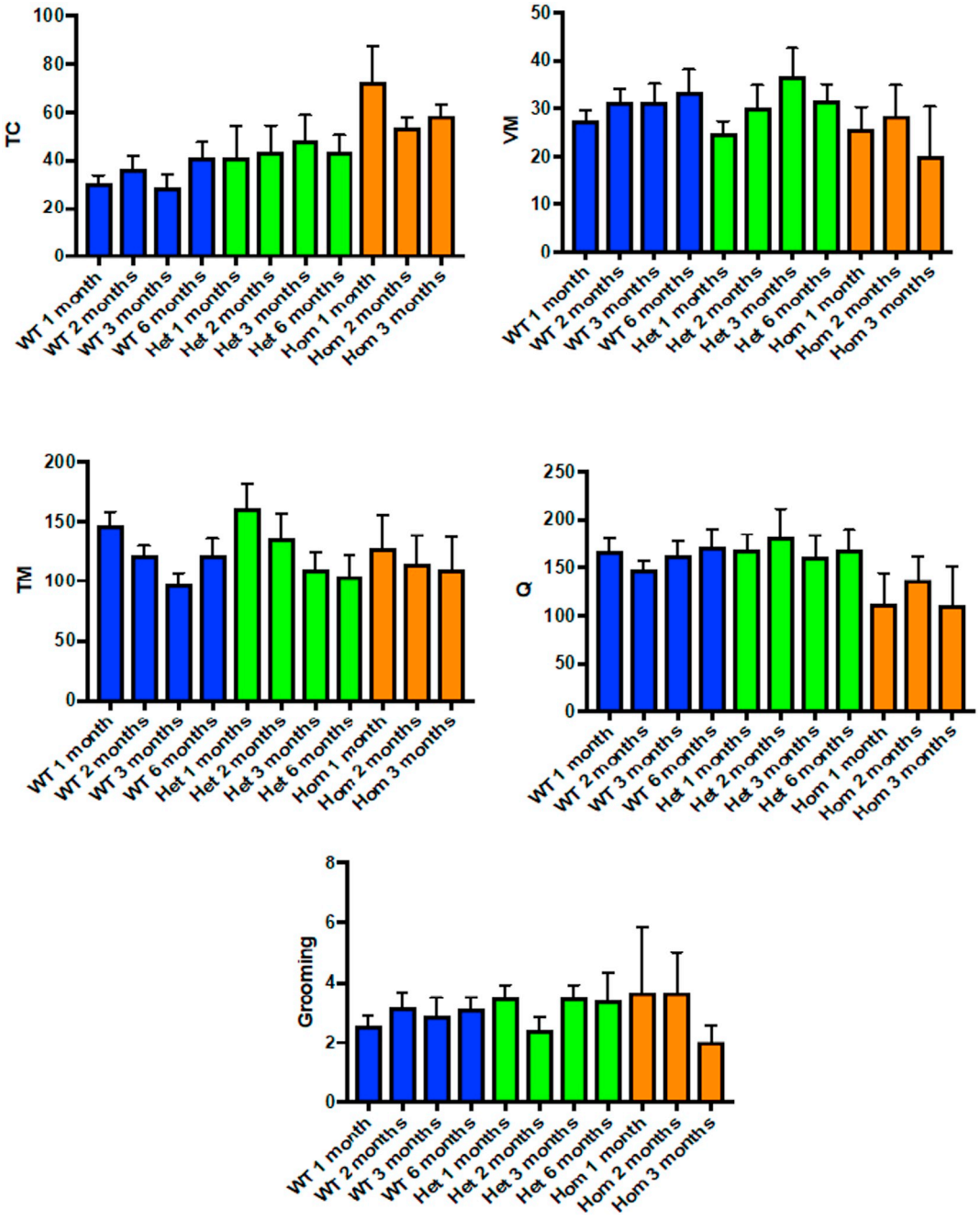

Fig. 10. Open Field Tests. Bars and boxes graphs representing wild type (WT) mice at 1 (n = 17), 2 (n = 17), 3 (n = 17), 6 (n = 9) months of age, heterozygous (Het) mice a 1 (n = 8), 2 (n = 7), 3 (n = 6), 6 (n = 5) months of age, and homozygous (Hom) at 1 (n = 3), 2 (n = 3) and 3 (n = 3) months of age. TC = time spent at the center; VM = vertical movements; TM = time spent moving; Q = numbers of quadrant crossed. Time is expressed in seconds.

walls, as can be seen in Fig. 10, this phenomenon being referred to as thigmotaxis (Kulesskaya and Voikar, 2014). Means of vertical activity (VM) for homozygous mice were lower than for WT or heterozygous mice. Old age groups are reported to exhibit reduction in vertical activity and center time compared with the younger (Shoji, 2016), accordingly, the time spent moving decreased with age in all groups independently from genotypes (Fig. 10), indicating that exploratory drive decreases with age. Center time and activity (together with defecation) in the first 5 min, likely measure some aspect of emotionality (Kulesskaya and Voikar, 2014).

The number of quadrants crossed is reported in Fig. 10 for each genotype and time point considered. Differences were not significant among time points for each genotype, nor among different genotypes at the same age. Studies on age-related changes in behavior in C57BL/6 revealed an age-dependent decline in locomotor activity (measured as distance travelled in cm) during the early testing period in a novel open field environment.

Such decrease was associated with an aging-dependent increased anxiety-like behavior rather than a decline in locomotor activity itself (Shoji, 2016). In our study mice were exposed at the same age to the same stimuli during their whole life, so getting used to the test procedure, allowing us to suppose that anxiety-like behaviors are limited. “Freezing” (standing still) was rarely seen, while grooming was quite common in all animals at any age, confirming in part that the bad conditions of the fur were not due to a decrease in the animal self-care. It's important to underline that despite standardization, OFT tests vary greatly across labs (Crabbe et al., 1999). Thus, experiments characterizing mutants may yield results that are tailored for a particular

Table 1
Numerical scoring system specific for Lmna^{G609G} transgenic mice. Grades were given always by the same operator. 3 = best condition possible; 10 = worst condition possible.

Parameter	Animal condition	Score
Fur	Shiny, thick, black	1
	Still in good condition, initial periocular alopecia	2
	Periocular alopecia, jagged, streaked, opaque and slightly greying fur	3
	General alopecia, thin, jagged, streaked, opaque fur	4
Gait analysis	Normal	1
	Unstable gait, divaricated hindlimbs	2
Activity	Active, lively, curious, jumps, runs, digs the litter	1
	Active, lively, does not jump, alternates time spent moving with increasing rests	2
	Active but not particularly lively, moves slowly	3
	Tends to stay still, trembles and is hypoactive	4
Total score		

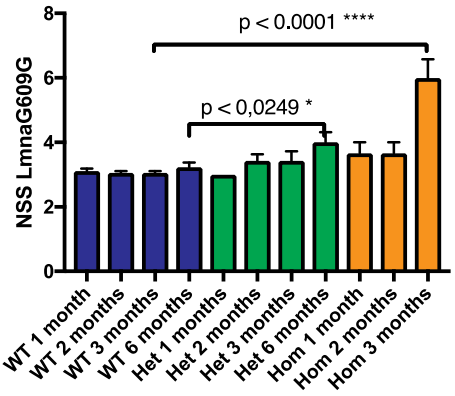

Fig. 11. Health condition description. Numerical scoring system used to describe the health.

laboratory being comparable intra- but not inter-lab.

2.9.2. Numerical scoring system specific for Lmna^{G609G} transgenic mice

Heterozygous mice at 6 months of age and homozygous mice at 3 months of age are smaller than WT littermates, have marked kyphosis, show prematurely aged fur but they still act in a way comparable to WT siblings. Objective indices of phenotypic alterations can be useful in following the progression of a disease. Based on this consideration we propose a numerical scoring system (NSS) specific for *Lmna*^{G609G} transgenic mice that gives values (from the best to the worst condition possible, 3 to 10) considering parameters such as fur, gait and activity (Table 1, Fig. 11).

conditions of *Lmna*$^{+/+}$, *Lmna*$^{G609G/+}$ at 1, 2, 3 and 6 months of age and of *Lmna*$^{G609G/G609G}$ at 1, 2 and 3 months of age.

This assessment revealed to be fast and easy to use. As it can be seen from the scores given after each OFT, WT mice had a nice fur, were active and walked normally until the last observation (6 months of age). This was not true for transgenic mice. *Lmna*$^{G609G/+}$ did not show much difference from WT mice up to 3 months of age. At 6 months, the NSS was significantly higher in *Lmna*$^{G609G/+}$ (p = 0.0249). The final score was influenced especially by the fur and skin conditions. However, at 6 months of age they still were very active. *Lmna*$^{G609G/G609G}$ were more severely affected and at 3 months of age already reached a mean score of 6. Again, the final score was influenced especially by the fur and skin conditions.

2.10. Skeletal abnormalities and radiological examinations

The acquisition of an abnormal posture (hunched-up) and kyphosis characterized this mouse model of progeria, as already reported by (Osorio et al., 2011). Kyphosis was also observed by in vivo clinical observations (Fig. 7), and during necroscopy. The seriousness and the onset of this feature depended on age and genotype (Fig. 12).

No WT animals had relevant radiological alterations up to 300 days of age, Kyphosis Index (KI) means were always above 4, and incisors were always normal (Fig. 12A, B, C, D). KI indexes of the heterozygous mice at weaning (30 days) were comparable to WT mice (Fig. 12B, C), differently from homozygous (Fig. 12B, C).

Kyphosis index for heterozygous mice was significantly lower than for WT mice starting from 200 days of age (p = 0,0152). The KI progressively got worse throughout the life of heterozygous (Fig. 12B, E1), in particular, during the last months of life this condition was extremely amplified (Fig. 12B, E2). Homozygous mice showed precocious and severe kyphosis. The deformity was always at the level of the chest stretch (Fig. 12B, C, F).

Abnormalities of the incisors were common. The lower incisors presented progressively a more flattened profile while the upper incisors showed an abnormal curvature with consequent malocclusion (Fig. 12G). No differences in kyphosis nor in the skull were evidenced between sexes of same genotype and age. Reduction of the abdominal fat was also evident in radiographs of transgenic mice, according to the genotype and age. Kyphosis arising during human normal aging is often related to osteoporosis through deformity of the vertebral bodies (Cummings and Melton, 2002), or to annulus degeneration (Resnik, 2002). Furthermore, humans affected by a reduction of vertebral mechanical support develop thoracic-lumbar spine deviation in a ventral/dorsal direction (lordosis or kyphosis), or a lateral deviation of the spine (scoliosis), due to gravity forces. In mice, conditions such as neuromuscular weakness would result in development of only kyphosis, due to the quadrupedal gait (Laws and Hoey, 2004). Cervical-thoracic kyphosis is reported in patients with HGPS (Hennekam, 2006). The early onset of spinal deformity in *Lmna*^{G609G} transgenic mice is likely attributable to osteoporosis, being causally similar to what happens in normal aging. However, in several transgenic mice, kyphosis was linked to osteosclerosis (Dabovic et al., 2002), growth plate abnormalities (Iba et al., 2001), muscular disorders (Burkin et al., 2001), compression or fractures. In our study, radiograph resolution was not sufficient to assess the presence of such changes that cannot therefore be excluded. As a first conclusion, the overall signs we could observe, related to the mutation, were evident in both genotypes, which represent reliable models of HGPS. In addition, the fairly milder phenotype of *Lmna*$^{G609G/+}$ mice, compared to *LMNA*$^{G608G/+}$ HGPS patients, is in agreement with a higher tolerance in mice to accumulation of prelamin A forms, compared to humans (Osorio et al., 2011).

2.11. Euthanasia

Animals were euthanized in the case they reached a total score of 10 or if one of the signs was evaluated with score 4 according to the Humane Endpoints table (HE) (Table 2). Euthanasia was carried out by an overdose of inhaled anesthetic (isoflurane 4% in O_2) in an induction chamber.

2.12. Post-mortem examinations

2.12.1. Pathological/histological observations

Tissues were surveyed at autopsy and by microscopic analysis. Some alterations confirmed the in vivo observations, such as the size reduction, the moderate to severe kyphosis in the first thoracic vertebrae, a generalized loss of fat deposits, the presence of alopecic areas and dental malocclusion for all *Lmna*^{G609G} transgenic mice. The most frequently affected organs were lung, skin, aorta, spleen, bones. Interstitial pneumonia (5/7 WT, 22/27 heterozygotes, 7/8 homozygotes) and hypoplasia/atrophy of the spleen lymphoid tissue (1/15 WT, 6/37 heterozygotes, 3/7 homozygotes) were non-specific changes observed in

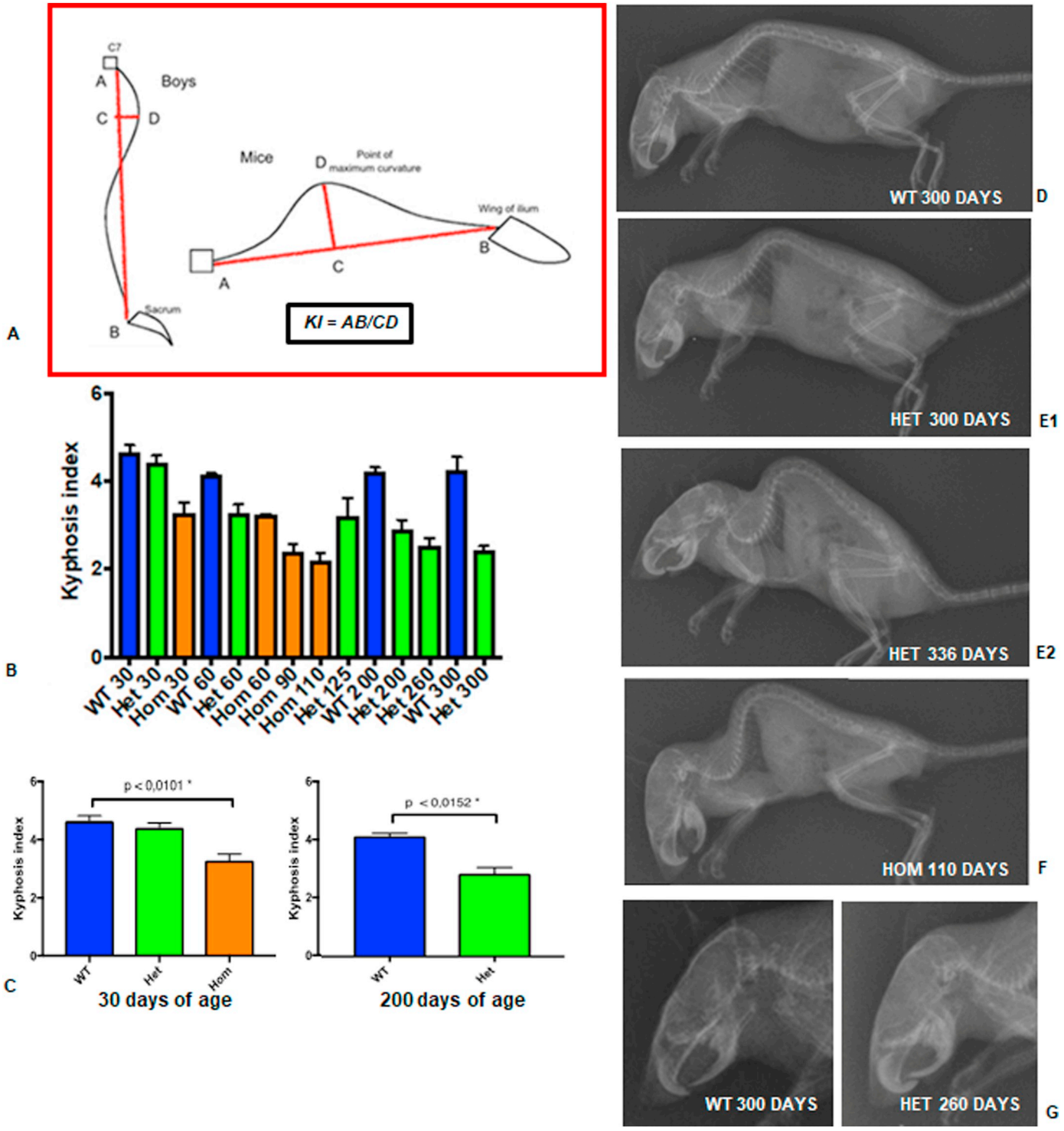

Fig. 12. Kyphosis. A) Kyphosis Index (KI) calculation method in humans and in mice; KI = AB/CD (adapted by (Laws and Hoey, 2004) B) KI assessment for wild type mice (WT), heterozygous (Het) and homozygous (Hom) mice, at different ages expressed in days. Severity of kyphosis depends on age and genotype. C) KI of wild type mice (n = 4), heterozygous (n = 5) and homozygous (n = 3) $Lmna^{G609G}$ transgenic mice at 30 days of age (left) and KI of wild type mice and heterozygous at 200 days of age (right). D) X-ray lateral projection of a wild type mice at 300 days of age. Note the normal anatomy of the mouth and disposition of the incisors. Abundant adipose tissue is present in the abdomen. E1, E2) X-ray lateral projection of the same heterozygous mice at 300 days and 336 days. KI index went in 36 days from 2.52 to 1.60. F) lateral projection a homozygous mouse at 110 days. G) Dental anomalies. X-ray lateral projection of the skull of a WT mouse at 300 days of age compared with a heterozygous mice at 260 days of age showing abnormalities of the incisors: the lower incisors grow towards the palate because of malocclusion.

all genotypes, while skin and aortic arch revealed to represent genotype-associated tissue targets when the severity of the lesions were appropriately graded as shown in Figs. 13–14.

In WT mice moderate skin alterations (grade 3 in the grading system described above) were observed at low frequency (3/14). In one case there was a moderate hypoplasia of the lymphoid tissue in spleen (not shown). No appreciable alterations at the level of the aorta were observed (0/7). In all cases the arteries graded 1.

Table 2
Humane endpoints. Total scores: 0–4: normal; 5–9: daily monitoring necessary; 10: animal with initial distress signs; 11–13: animal with distress signs; ≥14: severe distress.

Parameter	Animal conditions	Points
Feature	Normal	0
	Poor personal hygiene (grooming) index of mild depression of the sensorium	1
	Matted fur	2
	Significant loss of fur, curved posture	3
	Lateral or abdominal decubitus or limb/limbs paralysis	4
Intake of food and water	Normal - unknown: body weight < 5%	0–1
	Total anorexia: body weight < 15%	2
	Cachexia; poor general condition and evident weight loss	3
Respiratory symptoms	Normal respiratory rate	0
	Slight alteration of respiratory rate	1
	Increased respiratory rate and abdominal breathing	2
	Decreased respiratory rate speed and abdominal breathing	3
	Marked abdominal breathing and cyanosis	4
Spontaneous behavior	Normal	0
	Slight alterations; excitability	1
	Decreased mobility and alert; solitary confinement; relative inactivity	2
	Restless or very still; compulsive behaviors; repeated circular movements (circling) as index of possible brain suffering	3
Induced behavior	Normal	0
	Mild sensorium depression or exaggerated response to stimuli (auricle or pinch in footpad tests)	1
	Moderate changes in typical behavior	2
	Violent or extremely low reaction	3
Additional parameters	Rotated ears outwards and/or back; sharpened snout; narrow and half-closed eyes	4
	Rapid weight loss and severe dehydration	4
Total score		

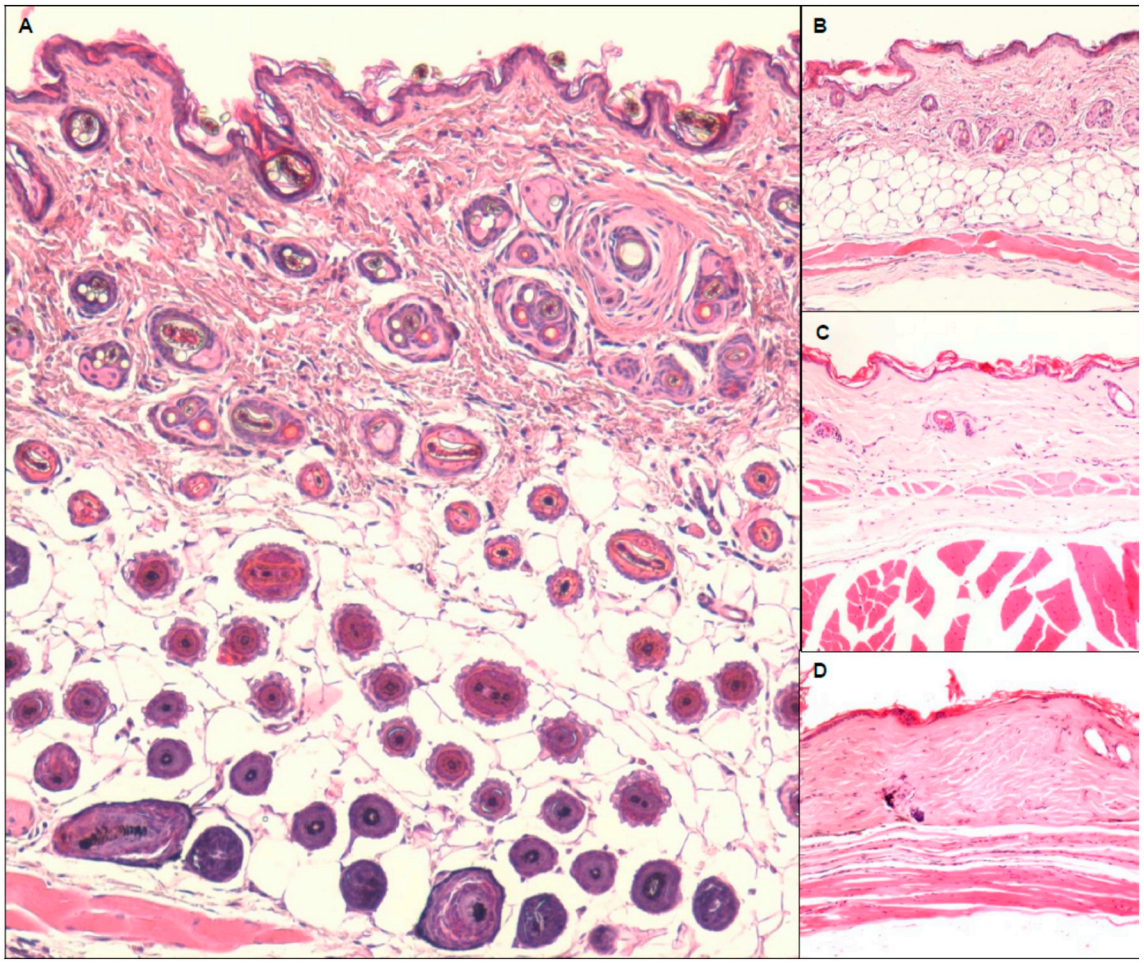

Fig. 13. Skin/subcutaneous adipose tissue atrophy grading. Haired skin. A Grade 1: normal skin with abundant subcutaneous adipose tissue and numerous hair follicles in the dermis and subcutis. B Grade 2: normal abundant adipose tissue and decreased hair follicles in both dermis and subcutis. C Grade 3: moderate atrophy of adipose tissue and scant hair follicles in the dermis. D Grade 4: severe atrophy/absence of adipose tissue in subcutis and of adnexa in the dermis. H&E; A: 200×, B, C, D: 100×.

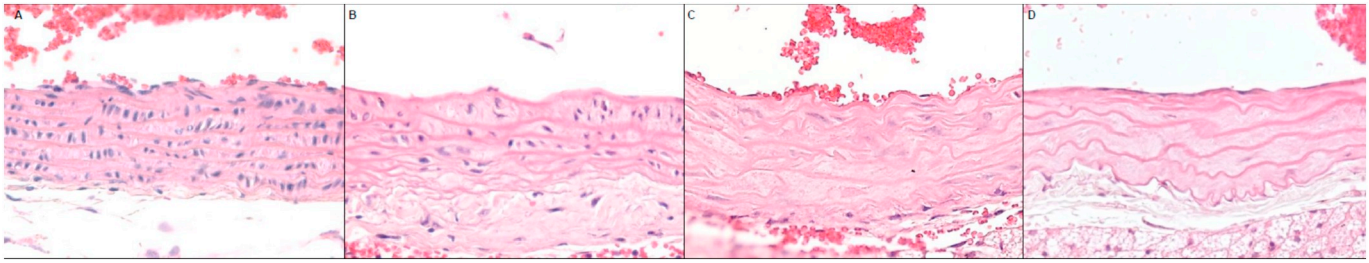

Fig. 14. Aortic arch-medium layer alteration grading. Increasing severity represented from left to right. A) Grade 1: normal aortic wall. B) Grade 2: mild decrease of cellularity and myxoid changes in middle coat (medium layer). Outer coat (adventitia layer) is normal. C) Grade 3: moderate decrease of cellularity and mild myxoid changes in middle coat. D) Grade 4: severe decrease of cellularity (almost absent) and severe myxoid changes in the middle coat extending to the outer coat. (H&E; 400×). Sections of aortic arch were also stained with periodic acid–Schiff (PAS) and Alcian at pH 2.5 and 1 to characterize the basophilic material (myxoid changes) (Fig. 15) collected in the medium layer in association with a reduction in the number of leiomyocytes.

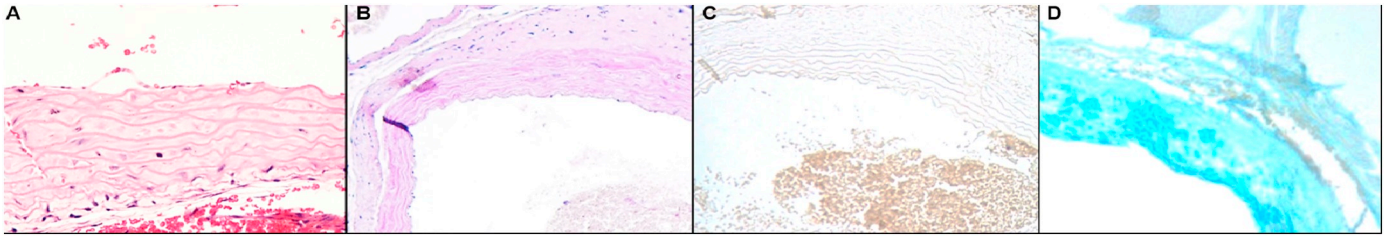

Fig. 15. Aortic arch from a $Lmna^{G609G/+}$ mouse. (A) In medium layer the interstitium is expanded by an homogeneous slightly eosinophilic material that stains negatively with PAS (B) and Alcian at pH 1 (C) but positive with Alcian at pH 2,5 (D) revealing to be non-sulphated acid mucins. A: 400×; B, C, D 100×.

Forty-seven $Lmna^{G609G/+}$ transgenic mice were examined. All had kyphosis, alopecia and dermal fibrosis, with reduction in number of hair follicles, that were mainly in the catagen phase. Regarding skin alterations, using the grading system described above (Fig. 13), in 47 heterozygotes one was graded 2, ten graded 3 and thirty-six graded 4. Regarding the aortic arch wall, alterations were present in 38 cases with reduction in the cell number, in the thickness of the *tunica media* and with multifocal accumulation of weakly basophil material, likely mucopolysaccharides. Using the grading system (Fig. 14) in heterozygotes, one artery resulted graded 1, ten arteries graded 2, fifteen graded 3 and twelve graded 4.

Nine $Lmna^{G609G/G609G}$ transgenic mice were examined. All had kyphosis Regarding skin alterations, alopecia, with reduction in number of follicles, and dermal fibrosis, were seen in 8/9 subjects. Using the grading system (Fig. 13), one animal was graded 2, two graded 3 and five graded 4. The subcutaneous fat was completely missing in all animals. Regarding the aortic arch wall, alterations were present in all animals. Eight aortas were available, one of which was graded 1, three graded 3 and four graded 4 (Fig. 14). The grading system for skin and aorta lesions revealed significant differences ($p < 0.001$) between both transgenic animals and $Lmna^{+/+}$, but not between $Lmna^{G609G/+}$ and $Lmna^{G609G/G609G}$ (Fig. 16).

Important cardiovascular alterations in terms of vascular smooth muscle cells at the level of the medial layer of the aortic arch were reported in $Lmna^{G609G/G609G}$ transgenic mice (Osorio et al., 2011; Balmus et al., 2018) together with alteration of the heart ventricular depolarization. However, these alterations were not graded nor evaluated for heterozygous mice. A recent study evidenced characteristic alterations at the aortic arch, which extend to the lower descending tract and to the carotids and subclavian arteries (Kim et al., 2018). A generalized increased stiffness of the aorta is also characteristic of the G609G mice, depending on increased collagen secretion in the medial layer together with smooth muscle cell loss (Del Campo et al., 2019) (Balmus et al., 2018) (Beyret et al., 2019).

A reported vascular calcification in $Lmna^{G609G}$ mice was attributable to reduced accumulation of pyrophosphate resulting from an increased, non-tissue-specific alkaline phosphatase activity and from a diminished ATP availability caused by mitochondrial dysfunction in vascular smooth muscle cells (Villa-Bellosta et al., 2013). Premature death of $Lmna^{G609G}$ transgenic mice could be linked to the cardiovascular alterations found, which also occur in HGPS patients and during normal aging. However, other causes, such as malnutrition, with consequent

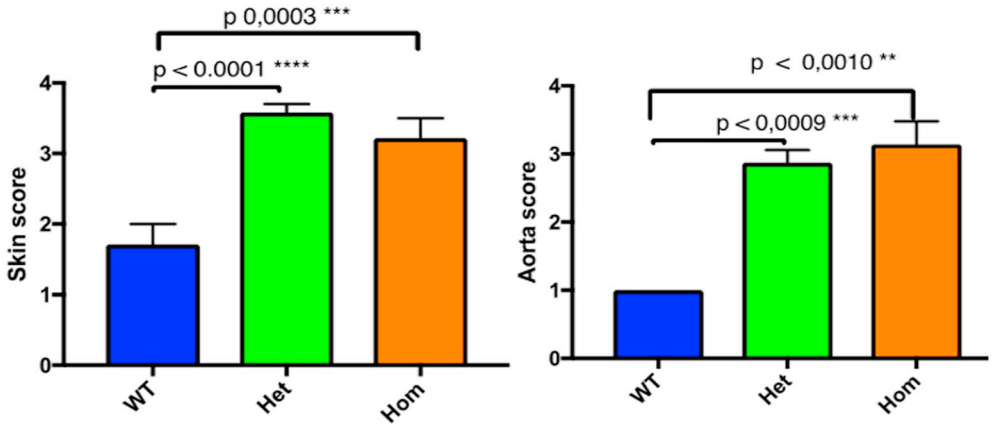

Fig. 16. Skin and aortic arch grading scores. Evaluation of transgenic animals who were sacrificed because they had reached the humane endpoint (about 108 days and 287 days for homozygous and heterozygous, respectively) and of wild type mice at about 280 days (controls). Differences between transgenic and wild type mice were significant, but not between heterozygous and homozygous mice.

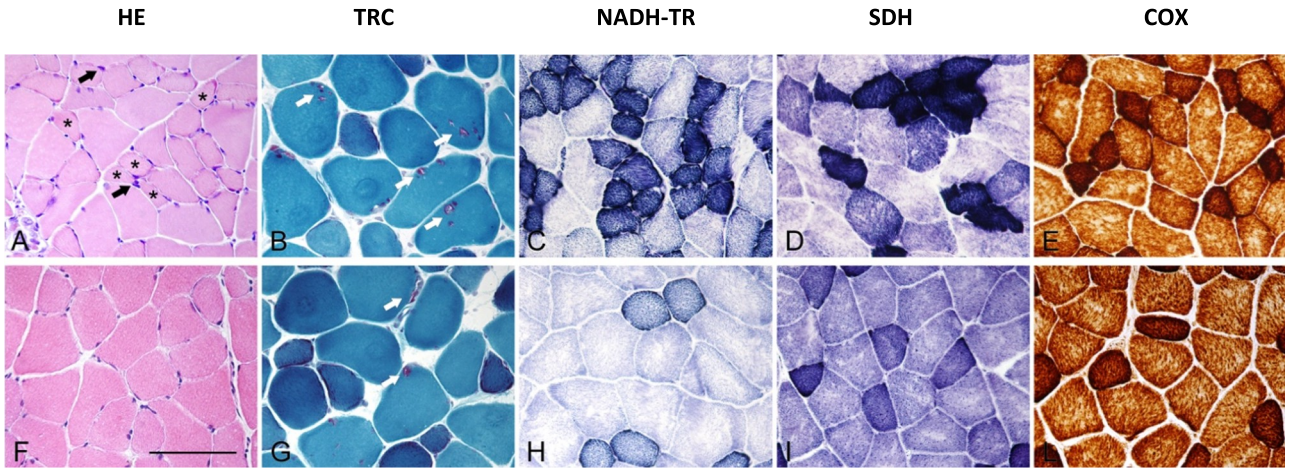

Fig. 17. Skeletal muscle histology. A–E = *Lmna*$^{G609G/+}$; F–L = WT. (A, F): *Lmna*$^{G609G/+}$ (A) show severe fiber atrophy (asterisks) and multifocally endomysial infiltrates of lymphocytes (arrow) compared to WT (F) (Hematoxylin/eosin). (B, G): *Lmna*$^{G609G/+}$ (B) shows more frequent intrasarcoplasmatic rimmed vacuoles (arrow) compared with WT (G) (Engel's Trichrome). (C, H): ragged blue fibers are more frequent in *Lmna*$^{G609G/+}$ (C) compared to WT (H) (Nicotinamide adenine dinucleotide tetrazolium reductase stain). (D, I): *Lmna*$^{G609G/+}$ (D) show more frequent ragged blue fibers compared to WT (I) (Succinate dehydrogenase stain). (E, L): *Lmna*$^{G609G/+}$ (E) show numerous fibers with "moth-eaten" appearance (cytochrome oxidase stain) (bar = 100 μm). (For interpretation of the references to color in this figure legend, the reader is referred to the web version of this article.)

possible decreased resistance to infective agents cannot be excluded. In this sense, the use of sterile caging for LmnaG609G transgenic mice is recommended as a preventive strategy.

2.12.2. Skeletal muscle histology

Skeletal muscle alterations have not been described in the human HGPS. Nevertheless LAMA/C mutations cause definite forms of muscle diseases, such as Emery-Dreifuss muscular dystrophy type 2 and 3, Limb-Girdle muscular dystrophy 1B, etc. Hence, we investigated if the G609G murine model of HGPS could develop skeletal muscle impairment. For describing the possible alterations in this tissue at the histological level, samples of quadriceps femoris muscle were collected from 16 *Lmna*$^{G609G/+}$ mice (8 males and 8 females), which mirror the heterozygous condition of the human syndrome, and from 14 WT (8 males and 6 females), ranging from 2 and 7,5 months of age (Fig. 17). Hematoxylin/eosin and Engel's Trichrome (TRC) stains of the *Lmna*$^{G609G/+}$ mice muscles showed mild to severe fiber atrophy compared to WT ($p < 0{,}0001$) (Fig. 17A). *Lmna*$^{G609G/+}$ mice showed more frequently rimmed vacuoles compared with WT but the difference was not significant ($p = 0{,}5091$). In *Lmna*$^{G609G/+}$, rare fibers showed centralized plump nuclei and rare pyknotic nuclear clumps. The endomysium showed multifocal lymphocyte infiltrates and few plasma cells (Fig. 17A, B, F, G). Inflammation was more severe in *Lmna*$^{G609G/+}$ subjects compared to WT ($p < 0{,}0001$) (Fig. 18). NADH-TR showed an irregular inter-myofibrillar network pattern (coarse appearance) in the vast majority of the fibers both in *Lmna*$^{G609G/+}$ and WT. In *Lmna*$^{G609G/+}$, NADH-TR and SDH showed numerous fibers with an intense and irregular subsarcolemmal staining (ragged blue fibers) (Fig. 17C, D, H, I) and COX showed numerous fibers with an irregular intermyofibrillar network ("moth-eaten" appearance) (Fig. 17 E, I). Mitochondrial alterations were more severe in *Lmna*$^{G609G/+}$ mice compared to WT ($p < 0{,}0001$) (Fig. 18). *Lmna*$^{G609G/+}$ mice showed a correlation between atrophy and age ($r^2 = 0{,}3718$; $p < 0{,}05$) which was not observed in the WT mice ($r^2 = 0{,}007671$; $p = 0{,}7659$) (Fig. 18).

According with other progeroid models (Greising et al., 2012), muscles of Lmna$^{G609G/+}$ mice have some of the key characteristics of sarcopenia, such as muscle atrophy and mitochondrial dysfunctions, which could result in weakness. Moreover, the observed inflammatory infiltrate could reflect a widely described chronic low-grade systemic inflammation associated with sarcopenia and called "inflammaging" (Costagliola et al., 2016).

2.12.3. Craniofacial skeleton alteration

Individual bony elements are conserved between mouse and human skulls. Analysis of the craniofacial skeleton of *Lmna*^{G609G} transgenic mice using μCT scans helps establishing parallels in human and mice phenotypes resulting from the same genetic alteration. Transgenic mice had abnormal skull shape. The bone reliefs were less marked and the indentations of the sutures between cranial bones were morphologically reduced in heterozygous and homozygous mice compared to WT ones. Transgenic mice also had micrognathia (small mandible) causing malocclusion. The consequence of such micrognathia is that mutant mice showed anomalies both in implantation and morphology of the incisors. In particular, upper incisors had an increase of the curvature (reduced

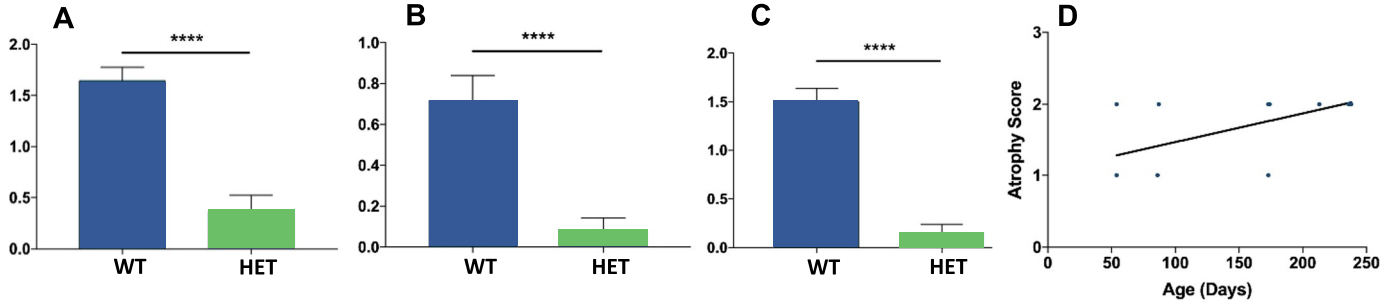

Fig. 18. Evaluation of skeletal muscle alterations. A) atrophy-, B) inflammation-, C) mitochondrial-alteration scores; A-B-C:****$P < 0.001$; D) atrophy-age correlation in *Lmna*$^{G609G/+}$; $r^2 = 0.37$; $P < 0.05$.

radius). The lower incisors of WT mice appeared triangular in shape by CT imaging, whereas in mutant mice they were cylindrical and showed a more flattened profile (Fig. 19). Interestingly the same alterations were described in a different prematurely-aging mouse model (*Zmpste24*$^{-/-}$) with impaired prelamin A processing to mature LamA/C (de Carlos et al., 2008).

2.12.4. Bone mechanical properties alteration

Human HGPS affects the skeletal system causing bone resorption and decreasing bone resistance, i.e. the capacity of bone segments to withstand loads (Gordon et al., 2011). Indeed, our experimental data, based on a four-point bending test, showed that the mechanical competence of mouse femurs was lower in Lmna$^{G609G/+}$ than in WT mice. A significant reduction of 40% and 33% was found in diaphysis stiffness and strength, respectively (Fig. 20A, B). This decrease is associated with a reduction in bone segment cross-section. Indeed, the cross-sectional dimension of Lmna$^{G609G/+}$ mouse femoral diaphysis was significantly lower than that of WT mouse: −24% and − 27% for cortical area and area moment of inertia, respectively (Fig. 20 C, D - for the sake of completeness, also the biomechanical length of Lmna$^{G609G/+}$ mouse femurs was on average 4% shorter than that of WT mice but the biomechanical length does not affect diaphysis stiffness and strength). A reduction in bone segment dimension had been already reported in the literature (Merideth et al., 2008) (Schmidt et al., 2012). However, the aforementioned changes in cross-sectional dimensions explain only partly the measured decrease in mechanical competence of the diaphysis. Indeed, microCT analyses showed an average reduction of 15% in mineralization of Lmna$^{G609G/+}$ mouse bone tissue. This finding is in agreement with the published observation that HGPS causes a decrease in bone tissue quality observed in a tissue-specific mouse model (Schmidt et al., 2012).

All these data suggest that the disease impacts on bone segments at

Fig. 19. MicroCT study of skulls. Top and lateral views. Surface renderings of μCT of the skull of a WT, a *Lmna*$^{G609G/+}$ and a *Lmna*$^{G609G/G609G}$ mice, respectively. The bone reliefs and the sutures between cranial bones were less marked in heterozygous and homozygous mouse compared to WT. In lateral view, micrognathia is observed in both transgenic mice as indicated with the red arrows. Micrognathia caused dental malocclusion. The red circle in the *Lmna*$^{G609G/G609G}$ mouse indicates an osteolytic lesion of the zygomatic arch. (For interpretation of the references to color in this figure legend, the reader is referred to the web version of this article.)

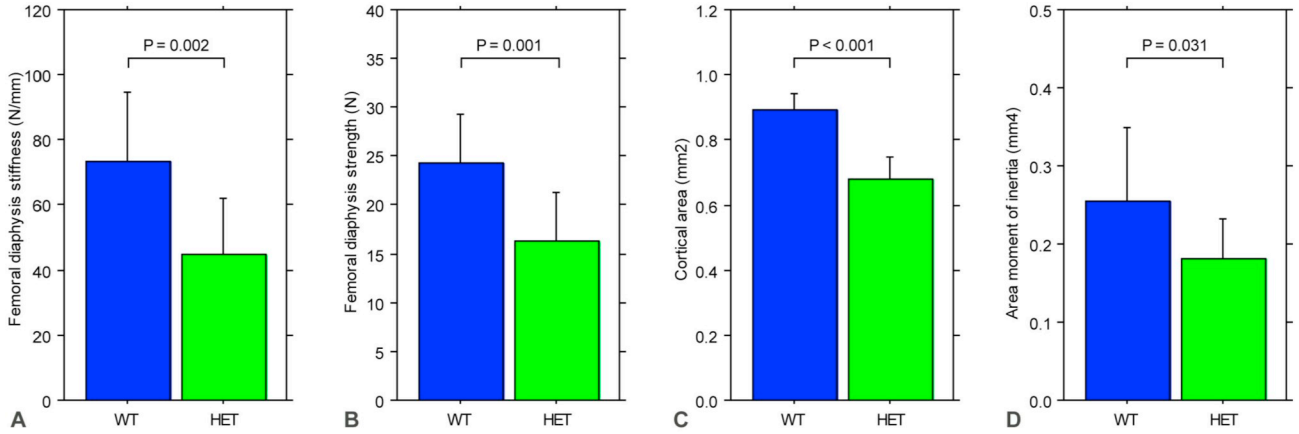

Fig. 20. Mechanical properties of the femoral diaphysis of WT and *Lmna*$^{G609G/+}$ mice. (A) Femoral diaphysis stiffness; (B) femoral diaphysis strength; (C, D) cross-sectional dimensions: cortical area (C) and area moment of inertia (D) of the femoral diaphysis.

two different scale levels: I) at tissue level, by decreasing both the ability to withstand load and the capacity to deform without fracturing; II) at organ level, by determining a diaphyseal cross-section morphology tinier than that found in WT mice. These detrimental results likely reflect the HGPS consequences on both metabolism and mechanotransduction mechanism of bone tissue. Indeed, it has been demonstrated that HGPS causes defect in bone matrix deposition and impacts on osteocyte distribution throughout the bone matrix (Schmidt et al., 2012) (Vidal et al., 2012). Whichever is the underlying mechanism, the assessment of mechanical competence of long bones retrieved from HGPS mice can supply additional quantitative evidence on the disease progression.

3. Conclusions

Detailed phenotypic data are increasingly described in studies dealing with animal models for human diseases and represent extremely important information when investigating longevity and comorbidities associated with aging. Given the highly conserved genome maintenance mechanism among species, mice can represent a valuable model for investigating genetic alterations, metabolic pathways and possible therapeutic strategies to address the aspects of human aging (Gurkar and Niedernhofer, 2015).

Reported mouse models engineered to mimic human HGPS may mirror the human phenotype in a partial manner, raising the question of the complexity of this disorder and the underlying mechanism. In this scenario, G609G mice engineered on a well-known genetic background (C57BL/6), represent a mouse model with a genetic mutation equivalent to that in human HGPS and allow scientists to describe and study in depth the pathophysiology of the human HGPS, hence planning possible therapeutic strategies. In addition, this model represents an outstanding tool for investigating the mechanism of normal aging (Osorio et al., 2011).

Our first goal was to define in detail the phenotype and breeding characteristics of *Lmna*^{G609G} transgenic mice. Both the homozygous and heterozygous genotypes were considered. This study represents the first description of this model over a long period (2 years), with special attention to reproduction, weaning, growth and expression of specific symptoms.

Homozygous mice were born with a lower frequency compared to what expected by Mendelian's proportion. They were not sterile but could not successfully deliver pups. On the contrary, heterozygous mice were successfully mated together, females being good breeders such as WT mice.

Both homozygous and heterozygous genotypes manifest most of the described human signs and symptoms: shorter life expectancy, reduced body growth, hair loss, absence of subcutaneous fat, dry skin, decreased mobility, skeletal and cardiovascular problems. Nevertheless, also differences are observed between human HGPS and G609G mice: e.g. periocular alopecia, microphthalmia, anophthalmia, opacity of the cornea appear only in mice, being never described in patients, who are reported to suffer mainly from refractive errors or pathologies related to corneal dryness (Merideth et al., 2008) (Mantagos et al., 2017) while nail dystrophy is observed in the human disease but not in G609G mice. Finally, skeletal muscle has not been studied in patients, hence alterations in this tissue have not been reported, but they are evident in mice (Table 3). Cardiovascular events are the first cause of death in humans. Although important alterations have been evidenced at the thoracic aorta level in mice, it is hard to establish if these are the basis of events leading to death of the animal. In fact, in parallel with the worsening of the signs, animals resulted malnourished and eventually they had to be euthanized because they reached the humane endpoint. As an example, malnourishment is largely prevented in patients, making this aspect of the disease course deeply different in the human syndrome.

Furthermore, we remark a significant difference between females and males in terms of weight trends and lifespan. In studies using this animal model, such differences should be kept in mind and groups of tested animals should be constructed accordingly.

It has been stated that homozygous mice represent the model of choice of human HGPS with respect to *Lmna*$^{G609/+}$ heterozygotes (Osorio et al., 2011). Our observations lead us to conclude that both homozygous and heterozygous animals represent a suitable model: the former shows signs of the disease really soon after weaning, making it difficult to test the efficacy and the safety of chronic treatments starting early in life, before symptoms may appear, while the distribution in time of any treatment may be more difficult because of the restricted lifespan; the latter would allow a more accurate evaluation of planned treatments although longer experimental time has to be considered because of the extended lifespan.

Whichever is the selected model, our description will help other research groups in choosing breeding strategies and mice housing, as well as in maintaining the focus on the signs and symptoms described as most characteristic of the mouse model and eliminating confounding signs deriving from the C57BL/6 genetic background. The outcomes of this study should represent, together with previously published data, the starting point for planning future researches on preclinical treatment trials.

Table 3
Comparison between G609G transgenic mice and human HGPS. HGPS patients are all heterozygotes *LMNA*$^{G608G/+}$. Mice are more tolerant than humans to accumulation of prelamin A forms and both heterozygous and homozygous survive. However, although the signs and symptoms are the same in heterozygous and homozygous mice, *Lmna*$^{G609G/G609G}$ are affected earlier in life compared to *Lmna*$^{G609G/+}$.

Feature	Human HGPS	*Lmna*^{G609G} transgenic mice
Growth	Severe growth deficiency. Kids are shorter and weight less	Severe growth deficiency in homozygotes, moderate in heterozygotes. Mice are smaller in size and weight
Hair/coat alterations	Balding, downy hair with the tendency to curl, absence of eyebrows and eyelashes, scarce or absent body hairs	Periocular alopecia and thin coat. Opaque and rough hair. Fur prematurely has grey stripes
Ocular alterations	Refractive errors, corneal dryness	Microphthalmia, anophthalmia, opacity of the cornea
Skin alterations	Moderate scleroderma; thick, thin, dry and atrophic skin; oedema	Dry, thin skin; erythema-like redness
Lipodystrophy	Expressed	Expressed
Cardiovascular alterations	vessel stiffness, vascular smooth muscle cell loss, adventitial thickening, and accelerated atherosclerosis, cardiac valves calcification	vessel stiffness, vascular smooth muscle cell loss, adventitial thickening, and accelerated atherosclerosis (only when expressed in an Apoe-null genetic background)
Mobility	Decreased Cervicothoracic kyphosis, scoliosis	Decreased Cervicothoracic kyphosis
Skeletal muscle alterations	Not reported	Age-related skeletal muscle atrophy associated with mild lymphocytic endomysial infiltrate and mitochondrial alterations.
Osseous apparatus		
Acra	Osteolysis of the distal phalanges; nails dystrophia	Undetectable
Clavicles	Narrow shoulders	Undetectable
Mandible	Retrognathia	Reduced and flattened mandible Micrognathia
Long bones	Osteoporosis	Reduced mechanical resistance, reduced mineralization
Viscerocranium	Small; decreased size of the maxilla and mandible with crowding of teeth	Micrognathia with dental malocclusion
Neurocranium	Mild; normal size dependent on the growth of the brain; vault relatively large compared to the face; delay in cranial suture closure	Normal skull size. Bone reliefs and the sutures between cranial bones are less marked
Lifespan	14.5 years	108 days homozygotes[a] 287 days heterozygotes[a]
Ratio females:males affected	No differences.	1:1.13 (homozygous) 1:1.53 (heterozygous)

[a] Significant differences among sex groups.

4. Materials and methods

4.1. HGPS mice model

The HGPS transgenic mice were a kind gift by Carlos-Lopez Otín, Departamento de Bioquímica y Biología Molecular, University of Oviedo (Spain). The knock-in mouse strain carrying the HGPS mutation was generated as described elsewhere (Osorio et al., 2011).

4.2. Housing and breeding

Breeding was conducted in compliance with the Italian Laws on animal experimentation in the Laboratory Animal Resources facility of the Department of Veterinary Medical Sciences-University of Bologna, starting from three *Lmna*$^{G609/+}$ progenitors (one male and two females, two-months old), after about a week for acclimatization. The mice received standard chow (Teklad 20/18 Rodent Diet, Envigo, Udine, Italy) and water ad libitum, were controlled daily and were weighed twice a week using a calibrated scale (Kern 440-47 N, Kern & Sohn GmbH, Balingen, Germany). Animals ate while grasping onto the wire cage top. A subset of these mice was fed also with moistened chow deposited on aluminum foils on the cage floor since the age of 2 month to assure feeding and weight maintenance to the less motile animals. Mice were maintained under a 12 h of dark/light life cycle at controlled temperature (20–24 °C) and humidity (40–70% RH). They were housed in conventional polycarbonate cages (Mouse Cage 1284L001, 365 mm L × 207 mm W × 140 mm H, Tecniplast, Varese, Italy) with same sex littermates. Average mice number per cage was 4, not segregated by genotype. The environmental enrichment (e.g. cardboard rolls, etc.) guaranteed the animals the opportunity to carry out the typical behavior of the specie.

Breeding pairs were housed together (2 females for each male) in bigger cages (Mouse Cage 1291H001, 425 mm L × 266 mm W × 185 mm H) from the age of 2–3 months until the age of 5–7 month and retired from reproduction before 1 year of age. Coupling f *Lmna*$^{G609/+}$ × m *Lmna*$^{G609/+}$ was preferred, however, in order to assure the maintenance of the strain we also coupled f WT × m *Lmna*$^{G609/+}$. Pups were kept with dams until an age of ~30 days to improve survival and at weaning they underwent sampling of the tail tip (for genotyping and progerin expression assessment) and headset marking (for identification) in deep general anesthesia.

4.3. Genotyping

DNA was extracted from tail tip fragments sampled under general anesthesia at weaning. Genomic DNA was isolated using Wizard Genomic DNA Purification kit (Promega, Italy), according to the manufacturer's recommendations. PCR was performed with published primers (Osorio et al., 2011) in a 25 µl volume containing 2.5 U AmpliTaq Gold DNA polymerase (ThermoFisher Scientific), 1× reaction buffer (10 mM Tris HCl pH 8.3, 50 mM KCl, 2.5 mM MgCl2), 200 µM of each deoxyribonucleoside triphosphate (dNTPs) and 0.2 mM each of primers using thermocycler (Model 9700; ThermoFisher Scientific). A 10 min denaturation step at 94 °C was followed by 35 cycles at 94 °C for 1 min, at 64 °C for 1 min, and at 72 °C for 1 min and completed by a final extension for 7 min at 72 °C. PCR products were purified by digestion with Antartic Phosphatase and Exonuclease I (New England BioLabs Inc.) and sequenced in both directions using Big Dye Terminator v3.1 Cycle sequencing kit (ThermoFisher Scientific) and applied onto DNA sequencer ABI Genetic Analyzer 3130 (ThermoFisher Scientific).

4.4. Western blot

LAMA/C and progerin amount in tail tip samples were evaluated by Western blotting analysis in 3 WT, 5 heterozygous and 5 homozygous mice. Proteins were extracted adding a lysis buffer containing 20 mM Tris–HCl, pH 7.5, 1% SDS, 1 mM Na3VO4, 1 mM PMSF, 5% β-mercaptoethanol and protease inhibitors. Tissue was sonicated and

centrifuged at 12,000*g* for 10 min at room temperature. The protein concentration was determined by Coomassie-blue staining and cellular extracts were boiled in SDS-containing sample buffer. Proteins underwent SDS gradient gel (6–20%) electrophoresis and transferred to a nitrocellulose membrane for 1 h. The membrane was saturated with 4% BSA in PBS plus 0.01% Tween 20 for 1 h and probed with anti-LAMA/C antibody (Santa Cruz Biotechnology N-18, 1:200 for 1 h). Bands were revealed by the Amersham ECL detection system.

4.5. Open Field Test

The Open Field Test (OFT) is widely used to measure locomotor activity and anxiety-like behavior (Prut and Belzung, 2003). A subset of mice underwent the OFT at 1, 2, 3, 6 and 9 months of age. A semi-transparent plastic white rectangular box (≈70 × 50 cm), was marked from underneath the surface with parallel lines both horizontal and vertical, forming a grid of 35 total quadrants, each measuring ≈9 × 9 cm. A central area of ≈39 × 23 cm was delimited. The arena was placed at the center of the room and illuminated at 100 lx. At the beginning of the test, each mouse was set in the middle of the arena and always the same two experienced operators during a 5 min period observed and recorded manually: travelled quadrants (Q), time spent moving (TM), time spent in the central area (TC), vertical movements (VM), freezing (F), grooming (G), feces (C) and urines (U). The operators were positioned as far as possible from the arena and remained still and quiet throughout each trial. The room was isolated from sound and unintentional interruptions were firmly avoided.

4.6. Radiological examinations

The radiographic study was performed in anaesthetized living animals using a human radiographic system (VILLA GENIUS HF, Italy) and Digital Radiography (DRX-Transportable, Carestream). Mice were placed in lateral recumbency and a single radiograph right lateral view of the whole body was obtained. Optimum exposure was established at 50 kV with 1.8 mAs with a film focal distance of 100 cm. Heterozygous mice were radiographed at 30, 60, 125, 200, 260 and 300 days of age and homozygous mice at 30, 60, 90 and 110 days of age. The images were recorded in DICOM format and then transferred to a personal computer. Kyphosis Index (KI, according to what is already reported by Laws and Hoey, 2004) and abnormalities of the skull (in particular the incisive teeth) were evaluated.

4.7. Anesthesia and Euthanasia

Deep general anesthesia conditions were obtained using 2.5% isoflurane in O_2 an anesthetic machine (Surgivet, Smith Medical Vet Division, Isotec 4 + LFY-1-A Medical Oxygen Concentrator, Biological instruments, Besozzo, Varese, Italy). Animals were euthanized when they reached a total Humane Endpoints (HE, Table 2) score of 10 or if one of the signs was evaluated with score 4. The procedure was carried out by administering an overdose of inhaled isoflurane (4% in O_2) in an induction chamber.

4.8. Pathological observations

Complete necropsies were performed in 70 mice (14 WT, 47 heterozygous, 9 homozygous) when reached the HE, i.e.: at about 108 days and 287 days for homozygous and heterozygous, respectively. Samples collected from skin (from interscapular and abdominal regions), lung, heart, aortic arch, spleen, kidney, liver, brain, vertebrae and femur were fixed with formalin and embedded in paraffin. Histology was based on hematoxylin-eosin stained sections and, for aorta, also on PAS stain (Bio Optica, Milan, Italy; P.A.S. Hotchkiss - MC Manus, 04-130802) and Alcian stains at pH 2,5 and 1 (Bio Optica, Milan, Italy, Alcian Blu, 04-160802).

Skin grading:

Grade 1: normal skin.

Grade 2: slight skin lesion. Normal abundant adipose tissue and decreased hair follicles in the dermis, associated to reduction of hair bulbs in subcutis.

Grade 3: moderate skin lesion. From moderate atrophy to absence of adipose tissue and scant telogen hair follicles in the dermis.

Grade 4: severe skin lesion. Almost absence of adipose tissue in subcutis and of adnexa in the dermis showing fibrosis.

Aorta arch grading:

Grade 1: normal aortic arch.

Grade 2: slight changes. Mild decrease of cellularity (up to 25%) associated to myxoid change in middle coat (media layer) without outer coat (adventitia layer) involvement.

Grade 3: moderate changes. Moderate decrease of cellularity (up to 50%) associated to myxoid change in middle coat without outer coat (adventitia layer) involvement.

Grade 4: severe changes. More than 50% decrease of cellularity associated to myxoid change, this latter extending from the middle to the outer coat (adventitia layer).

4.9. Skeletal muscle histology

Quadriceps femoris were collected from 30 animals, 16 $Lmna^{G609G/+}$ mice, 8 males and 8 females and 14 WT, 8 males and 6 females, ranging from 2 and 7,5 months of age.

Muscle samples were snap frozen in isopentane pre-cooled in liquid nitrogen. Transverse sections (8 μm thick) were cut at −20 °C and stained with: a) hematoxylin-eosin and Engel trichrome for a basic morphologic evaluation and mitochondria distribution; b) reduced nicotinamide-adenine-dinucleotide tetrazolium-reductase to evaluate the distribution of mitochondria and sarcoplasmic network; c) succinate-dehydrogenase and d) cytochrome oxidase to evaluate distribution and activity of mitochondria. The severity of atrophy, inflammation, vacuolization and mitochondrial damage were scored as 0 = absent; 1 = mild; 2 = moderate; 3 = severe. Statistical analysis was performed with IBM SPSS Statistics 25.0. The differences between LmnaG609G/+ and WT were evaluated with *t*-test and the correlations were evaluated with Pearson correlation coefficient.

4.10. Skeletal microCT

Whole heads, collected from 2 WT, 4 $Lmna^{G609G/+}$ and 4 $Lmna^{G609G/G609G}$ mice, were analyzed on a microCT model Skyscan 1072 (Bruker Corp., MicroCT unit, Kontich, Belgium) to investigate the craniofacial skeleton alteration. The samples were immersed in saline solution during scanning. The scanning parameters were set at a voxel resolution of 19.5 μm, 50 kV, 200 μA, 1 mm aluminum filter, exposure time 5936 ms, image averaged on 2 frames, rotation 180° and a rotation step of 0.9°. Tomographic image reconstruction was based on NRecon software (Bruker Corp., MicroCT unit, Kontich, Belgium). A global threshold was applied to select bone tissue (grey threshold value 117/255). Mouse heads were qualitatively analyzed on 3D reconstructions to identify any possible alteration in craniofacial skeleton, with particular attention to sutures, shape of mandible and incisors.

4.11. Evaluation of mechanical bone properties

At sacrifice of $Lmna^{G609G/+}$ mouse, one whole posterior leg was retrieved and immediately frozen at −20 °C. Thirteen legs were collected. Similarly, one posterior leg was also retrieved from thirteen age-matched WT mice.

At time of testing, the selected frozen leg was sealed inside a laboratory glove and thawed by immersion in 37 °C water for 5 min. The femur was cleaned from soft tissues and preliminary analyzed on a

microCT as described above (only voxel resolution was 10.8 μm instead of 19.5 μm). Cortical area and area moment of inertia in the mid-third region of the femoral shaft were determined on 3D reconstructions by use of Ctan software (Bruker Corp., MicroCT unit, Kontich, Belgium).

The femur underwent a four-point bending test to determine the diaphysis stiffness and strength in anterior-posterior direction, i.e. the sagittal anatomical plane, defined as the plane passing through the femoral axis and orthogonal to the line tangent to the posterior aspect of the femoral condyles. The femoral axis was defined as the line passing through the center of two cross sections located at 25% and 70% of the biomechanical length, i.e. the longitudinal distance between the cranial side of the intertrochanteric fossa and the intercondylar fossa. The two epiphyses of each femur were embedded into two square cross-sectional thin-walled pots to maintain the femur in the desired position during the bending test. All the tests were completed within 5 h from leg thawing. Collected data were analyzed using the Mann-Whitney test.

Acknowledgements

The Authors thank Carlos Lopez-Otín for providing the G609G mice.

Declaration of competing interest

No competing interests declared.

Funding sources

This work was supported by E-RARE project 2018–2021 “Exploring new therapeutic strategies in Hutchinson-Gilford progeria syndrome preclinical models” co-funded by Associazione Italiana Progeria Sammy Basso (A.I.Pro.Sa.B.).

MIUR (Italian Ministry for University and Research) PRIN 2016–2020: “Targeting autophagy in myogenic cells to counteract muscle aging and neuromuscular diseases: novel bioengineering tools for validating pharmacological candidates”.

References

Balmus, G., Larrieu, D., Barros, A.C., Collins, C., Abrudan, M., Demir, M., Geisler, N.J., Lelliott, C.J., White, J.K., Karp, N.A., Atkinson, J., Kirton, A., Jacobsen, M., Clift, D., Rodriguez, R., Adams, D.J., Jackson, S.P., S. M. G. Project, 2018. Targeting of NAT10 enhances healthspan in a mouse model of human accelerated aging syndrome. Nat. Commun. 9 (1), 1700.

Baumans, V., 2005. Science-based assessment of animal welfare: laboratory animals. Rev. Sci. Tech. 24 (2), 503–513.

Beyret, E., Liao, H.K., Yamamoto, M., Hernandez-Benitez, R., Fu, Y., Erikson, G., Reddy, P., Izpisua Belmonte, J.C., 2019. Single-dose CRISPR-Cas9 therapy extends lifespan of mice with Hutchinson-Gilford progeria syndrome. Nat. Med. 25 (3), 419–422.

van den Broek, F.A., Omtzigt, C.M., Beynen, A.C., 1993. Whisker trimming behaviour in A2G mice is not prevented by offering means of withdrawal from it. Lab. Anim. 27 (3), 270–272.

Burkholder, T., Foltz, C., Karlsson, E., Linton, C.G., Smith, J.M., 2012. Health evaluation of experimental laboratory mice. Curr Protoc Mouse Biol 2, 145–165.

Burkin, D.J., Wallace, G.Q., Nicol, K.J., Kaufman, D.J., Kaufman, S.J., 2001. Enhanced expression of the alpha 7 beta 1 integrin reduces muscular dystrophy and restores viability in dystrophic mice. J. Cell Biol. 152 (6), 1207–1218.

Camozzi, D., Capanni, C., Cenni, V., Mattioli, E., Columbaro, M., Squarzoni, S., Lattanzi, G., 2014. Diverse lamin-dependent mechanisms interact to control chromatin dynamics: focus on laminopathies. Nucleus 5 (5).

de Carlos, F., Varela, I., Germanà, A., Montalbano, G., Freije, J.M., Vega, J.A., López-Otin, C., Cobo, J.M., 2008. Microcephalia with mandibular and dental dysplasia in adult Zmpste24-deficient mice. J. Anat. 213 (5), 509–519.

Costagliola, A., Wojcik, S., Pagano, T.B., De Biase, D., Russo, V., Iovane, V., Grieco, E., Papparella, S., Paciello, O., 2016. Age-related changes in skeletal muscle of cattle. Vet. Pathol. 53 (2), 436–446.

Crabbe, J.C., Wahlsten, D., Dudek, B.C., 1999. Genetics of mouse behavior: interactions with laboratory environment. Science 284 (5420), 1670–1672.

Cummings, S.R., Melton, L.J., 2002. Epidemiology and outcomes of osteoporotic fractures. Lancet 359 (9319), 1761–1767.

Dabovic, B., Chen, Y., Colarossi, C., Obata, H., Zambuto, L., Perle, M.A., Rifkin, D.B., 2002. Bone abnormalities in latent TGF-[beta] binding protein (Ltbp)-3-null mice indicate a role for Ltbp-3 in modulating TGF-[beta] bioavailability. J. Cell Biol. 156 (2), 227–232.

De Sandre-Giovannoli, A., Bernard, R., Cau, P., Navarro, C., Amiel, J., Boccaccio, I., Lyonnet, S., Stewart, C.L., Munnich, A., Le Merrer, M., Lévy, N., 2003. Lamin a truncation in Hutchinson-Gilford progeria. Science 300 (5628), 2055.

Del Campo, L., Sánchez-López, A., Salaices, M., von Kleeck, R.A., Expósito, E., González-Gómez, C., Cussó, L., Guzmán-Martínez, G., Ruiz-Cabello, J., Desco, M., Assoian, R.K., Briones, A.M., Andrés, V., 2019. Vascular smooth muscle cell-specific progerin expression in a mouse model of Hutchinson-Gilford progeria syndrome promotes arterial stiffness: therapeutic effect of dietary nitrite. Aging Cell 18 (3), e12936.

Eriksson, M., Brown, W.T., Gordon, L.B., Glynn, M.W., Singer, J., Scott, L., Erdos, M.R., Robbins, C.M., Moses, T.Y., Berglund, P., Dutra, A., Pak, E., Durkin, S., Csoka, A.B., Boehnke, M., Glover, T.W., Collins, F.S., 2003. Recurrent de novo point mutations in lamin A cause Hutchinson-Gilford progeria syndrome. Nature 423 (6937), 293–298.

Fuerst, P.G., Rauch, S.M., Burgess, R.W., 2007. Defects in eye development in transgenic mice overexpressing the heparan sulfate proteoglycan agrin. Dev. Biol. 303 (1), 165–180.

González, J.M., Andrés, V., 2011. Synthesis, transport and incorporation into the nuclear envelope of A-type lamins and inner nuclear membrane proteins. Biochem. Soc. Trans. 39 (6), 1758–1763.

Gordon, C.M., Gordon, L.B., Snyder, B.D., Nazarian, A., Quinn, N., Huh, S., Giobbie-Hurder, A., Neuberg, D., Cleveland, R., Kleinman, M., Miller, D.T., Kieran, M.W., 2011. Hutchinson-Gilford progeria is a skeletal dysplasia. J. Bone Miner. Res. 26 (7), 1670–1679.

Greising, S.M., Call, J.A., Lund, T.C., Blazar, B.R., Tolar, J., Lowe, D.A., 2012. Skeletal muscle contractile function and neuromuscular performance in Zmpste24 −/− mice, a murine model of human progeria. Age (Dordr.) 34 (4), 805–819.

Gurkar, A.U., Niedernhofer, L.J., 2015. Comparison of mice with accelerated aging caused by distinct mechanisms. Exp. Gerontol. 68, 43–50.

Hamczyk, M.R., Villa-Bellosta, R., Gonzalo, P., Andrés-Manzano, M.J., Nogales, P., Bentzon, J.F., López-Otín, C., Andrés, V., 2018. Vascular smooth muscle-specific progerin expression accelerates atherosclerosis and death in a mouse model of Hutchinson-Gilford progeria syndrome. Circulation 138 (3), 266–282.

Hennekam, R.C., 2006. Hutchinson-Gilford progeria syndrome: review of the phenotype. Am. J. Med. Genet. A 140 (23), 2603–2624.

Iba, K., Durkin, M.E., Johnsen, L., Hunziker, E., Damgaard-Pedersen, K., Zhang, H., Engvall, E., Albrechtsen, R., Wewer, U.M., 2001. Mice with a targeted deletion of the tetranectin gene exhibit a spinal deformity. Mol. Cell. Biol. 21 (22), 7817–7825.

Kalueff, A.V., Minasyan, A., Keisala, T., Shah, Z.H., Tuohimaa, P., 2006. Hair barbering in mice: implications for neurobehavioural research. Behav. Process. 71 (1), 8–15.

Kim, P.H., Luu, J., Heizer, P., Tu, Y., Weston, T.A., Chen, N., Lim, C., Li, R.L., Lin, P.Y., Dunn, J.C.Y., Hodzic, D., Young, S.G., Fong, L.G., 2018. Disrupting the LINC complex in smooth muscle cells reduces aortic disease in a mouse model of Hutchinson-Gilford progeria syndrome. Sci. Transl. Med. 10 (460).

Kulesskaya, N., Voikar, V., 2014. Assessment of mouse anxiety-like behavior in the light-dark box and open-field arena: role of equipment and procedure. Physiol. Behav. 133, 30–38.

Laws, N., Hoey, A., 2004. Progression of kyphosis in mdx mice. J Appl Physiol (1985) 97 (5), 1970–1977.

Liao, C.Y., Anderson, S.S., Chicoine, N.H., Mayfield, J.R., Academia, E.C., Wilson, J.A., Pongkietisak, C., Thompson, M.A., Lagmay, E.P., Miller, D.M., Hsu, Y.M., McCormick, M.A., O'Leary, M.N., Kennedy, B.K., 2016. Rapamycin reverses metabolic deficits in lamin A/C-deficient mice. Cell Rep. 17 (10), 2542–2552.

Long, S.Y., 1972. Hair-nibbling and whisker-trimming as indicators of social hierarchy in mice. Anim. Behav. 20 (1), 10–12.

Lopez-Soler, R.I., Moir, R.D., Spann, T.P., Stick, R., Goldman, R.D., 2001. A role for nuclear lamins in nuclear envelope assembly. J. Cell Biol. 154 (1), 61–70.

Louis, E.D., 2008. Environmental epidemiology of essential tremor. Neuroepidemiology 31 (3), 139–149.

Mantagos, I.S., Kleinman, M.E., Kieran, M.W., Gordon, L.B., 2017. Ophthalmologic features of progeria. Am J. Ophthalmol. 182, 126–132.

Merideth, M., Gordon, L., Clauss, S., Sachdev, V., Smith, A., Perry, M., Brewer, C., Zalewski, C., Kim, H., Solomon, B., Brooks, B., Gerber, L., Turner, M., Domingo, D., Hart, T., Graf, J., Reynolds, J., Gropman, A., Yanovski, J., Gerhard-Herman, M., Collins, F., Nabel, E., Cannon, R., Gahl, W., Introne, W., 2008. Phenotype and course of Hutchinson-Gilford progeria syndrome. N. Engl. J. Med. 358 (6), 592–604.

Meta, M., Yang, S., Bergo, M., Fong, L., Young, S., 2006. Protein farnesyltransferase inhibitors and progeria. Trends Mol. Med. 12 (10), 480–487.

Moir, R.D., Spann, T.P., 2001. The structure and function of nuclear lamins: implications for disease. Cell. Mol. Life Sci. 58 (12−13), 1748–1757.

Mounkes, L.C., Stewart, C.L., 2004. Aging and nuclear organization: lamins and progeria. Curr. Opin. Cell Biol. 16 (3), 322–327.

Osorio, F.G., Obaya, A.J., López-Otín, C., Freije, J.M., 2009. Accelerated ageing: from mechanism to therapy through animal models. Transgenic Res. 18 (1), 7–15.

Osorio, F.G., Navarro, C.L., Cadiñanos, J., López-Mejía, I.C., Quirós, P.M., Bartoli, C., Rivera, J., Tazi, J., Guzmán, G., Varela, I., Depetris, D., de Carlos, F., Cobo, J., Andrés, V., De Sandre-Giovannoli, A., Freije, J.M., Lévy, N., López-Otín, C., 2011. Splicing-directed therapy in a new mouse model of human accelerated aging. Sci. Transl. Med. 3 (106), 106ra107.

Prokocimer, M., Barkan, R., Gruenbaum, Y., 2013. Hutchinson-Gilford progeria syndrome through the lens of transcription. Aging Cell 12 (4), 533–543.

Prut, L., Belzung, C., 2003. The open field as a paradigm to measure the effects of drugs on anxiety-like behaviors: a review. Eur. J. Pharmacol. 463 (1–3), 3–33.

Resnik, R., 2002. Intrauterine growth restriction. Obstet. Gynecol. 99 (3), 490–496.

Schmidt, E., Nilsson, O., Koskela, A., Tuukkanen, J., Ohlsson, C., Rozell, B., Eriksson, M., 2012. Expression of the Hutchinson-Gilford progeria mutation during osteoblast development results in loss of osteocytes, irregular mineralization, and poor biomechanical properties. J. Biol. Chem. 287 (40), 33512–33522.

Shoji, H., 2016. Scaling law in free walking of mice in circular open fields of various diameters. J. Biol. Phys. 42 (2), 259–270.
Smith, R.S., Roderick, T.H., Sundberg, J.P., 1994. Microphthalmia and associated abnormalities in inbred black mice. Lab. Anim. Sci. 44 (6), 551–560.
Vidal, C., Bermeo, S., Fatkin, D., Duque, G., 2012. Role of the nuclear envelope in the pathogenesis of age-related bone loss and osteoporosis. Bonekey Rep 1, 62.
Villa-Bellosta, R., Rivera-Torres, J., Osorio, F.G., Acín-Pérez, R., Enriquez, J.A., López-Otín, C., Andrés, V., 2013. Defective extracellular pyrophosphate metabolism promotes vascular calcification in a mouse model of Hutchinson-Gilford progeria syndrome that is ameliorated on pyrophosphate treatment. Circulation 127 (24), 2442–2451.
Weber, E.M., Algers, B., Würbel, H., Hultgren, J., Olsson, I.A., 2013. Influence of strain and parity on the risk of litter loss in laboratory mice. Reprod. Domest. Anim. 48 (2), 292–296.
Weber, E.M., Hultgren, J., Algers, B., Olsson, I.A., 2016. Do laboratory mouse females that lose their litters behave differently around parturition? PLoS One 11 (8), e0161238.